Development of KRAS-Targeting siRNA and Chemotherapy Co-Delivery Chitosan NPs for Enhanced Treatment of Pancreatic Cancer

Yu-Ting Chien

A thesis

submitted in partial fulfillment of the

requirements for the degree of

Master of Science

University of Washington

2025

Committee:

Miqin Zhang

Qingxin Mu

Program Authorized to Offer Degree:

Pharmaceutics

University of Washington

Abstract

Development of KRAS-Targeting siRNA and Chemotherapy Co-Delivery Chitosan NPs for Enhanced Treatment of Pancreatic Cancer

Yu-Ting Chien

Chair of the Supervisory Committee:

Miqin Zhang

Department of Materials Science and Engineering

Pancreatic ductal adenocarcinoma (PDAC) remains one of the most lethal cancers due to its aggressive progression, late-stage diagnosis, and limited treatment options. These clinical challenges are compounded by intrinsic resistance to chemotherapy and the high prevalence of activating mutations in the Kirsten rat sarcoma viral oncogene homolog (KRAS). To address these barriers, we developed a chitosan-based nanoparticle platform for the co-delivery of paclitaxel (PTX) and small interfering RNA (siRNA) targeting a prevalent KRAS variant, G12D (CP-PTX-KRAS G12D siRNA NPs) to pancreatic cancer cells. The CP-PTX conjugate was synthesized via carbodiimide-mediated coupling between pegylated chitosan and carboxyl-modified PTX, then complexed with siRNA through electrostatic interactions to form dual-functional NPs.

The optimized formulation exhibited a compact size (~26.5 nm) and a moderately negative zeta potential (−9.8 mV), indicating stable siRNA loading and favorable physicochemical properties

for intracellular delivery. The platform was initially validated using PolyIC, a double-stranded RNA and firefly luciferase siRNA to optimize formulation parameters and assess delivery efficiency. Cytotoxicity assays in KRAS G12D-mutant PANC-1 cells revealed dose-dependent viability reductions with single-agent PTX and KRAS siRNA, exhibiting IC50 values of 0.5470 μM and 0.2784 μM, respectively. Co-treatment at fixed PTX:siRNA molar ratios (1:0.2, 1:0.5, 1:1, 1:2) significantly enhanced cytotoxicity compared to single agents. CP-PTX-siRNA NPs achieved consistently lower total IC50 values than corresponding admix drug combinations across all tested ratios. At the 1:0.2 ratio, the NPs formulation showed a total IC50 of 0.0921 μM (vs. 0.1328 μM for free drug), with a CI value of 0.317, indicating strong synergy. Similar trends were observed for other ratios, with all CI values <1, supporting synergistic interactions between PTX and siRNA when co-delivered via NPs.

These findings demonstrate the potential of CP-PTX-siRNA NPs as an effective co-delivery platform for chemo-gene therapy in KRAS-driven pancreatic cancer. This system offers a modular and biocompatible approach to overcoming drug resistance and genetic drivers of malignancy, supporting its further development for translational cancer therapy.

Table of Contents

1. Introduction

1.1 Pancreatic Cancer and Main Characteristics

Pancreatic ductal adenocarcinoma (PDAC), representing the majority of pancreatic cancer cases, is among the most aggressive and treatment-resistant malignancies, with a five-year survival rate of just 12% in the United States (1). Its poor prognosis stems from late diagnosis, rapid progression, and limited responsiveness to conventional therapies. Most patients present with unresectable disease, and the tumor microenvironment—marked by dense fibrosis, poor vascularization, and immunosuppressive cells—further hinders drug delivery and immune response (2). Genetic mutations, particularly in *KRAS*, *TP53*, *CDKN2A*, and *SMAD4*, contribute to its aggressive biology and therapeutic resistance (3, 4). KRAS mutations, particularly common in PDAC, activate signaling pathways promoting cell proliferation, survival, and immune evasion (4). Most patients are diagnosed at advanced, often unresectable stages, severely limiting therapeutic options. Even for patients undergoing surgical resection—the only potentially curative approach—high recurrence rates persist due to undetected micrometastases and intrinsic drug resistance (5).

A major obstacle in treating PDAC is its unique tumor microenvironment, characterized by dense stromal fibrosis, limited vascularization, and profound immunosuppression (6). This fibrotic stroma, comprising extracellular matrix proteins, cancer-associated fibroblasts, and immunosuppressive cells like regulatory T-cells and myeloid-derived suppressor cells, significantly impedes drug delivery and dampens antitumor immune responses (7). Studies have demonstrated that drug delivery to PDAC tumors is markedly lower compared to other malignancies due to elevated interstitial pressure and the physical barriers created by dense fibrosis. Consequently, conventional chemotherapy agents achieve only limited accumulation within PDAC tumors, substantially reducing therapeutic efficacy (8).

1.2 KRAS Mutations in Pancreatic Cancer

KRAS mutations are among the most frequent and early occurring genetic alterations in PDAC, detected in over 90% of cases (9). These mutations play a pivotal role in driving tumor initiation, progression, and maintenance. The most common mutation is the G12D variant, resulting from a glycine-to-aspartate substitution at codon 12, which accounts for approximately 35–45% of all KRAS-mutant PDAC cases (10). This single-nucleotide substitution renders the KRAS protein constitutively active, leading to persistent signaling through downstream pathways such as RAF–MEK–ERK and PI3K–AKT, thereby promoting uncontrolled cell proliferation, survival, and resistance to apoptosis (Prior (11, 12). KRAS G12D also contributes to the immunosuppressive tumor microenvironment by modulating cytokine production and immune cell recruitment, further complicating treatment (13). Despite its central role in PDAC pathogenesis, KRAS has historically been considered "undruggable" due to its high affinity for GTP/GDP and lack of

accessible binding pockets. However, recent advances in RNA interference and allele-specific inhibitors have renewed interest in targeting KRAS as a therapeutic strategy (14, 15). Recent developments include small-molecule inhibitors like MRTX1133, which have demonstrated promising preclinical efficacy in mouse models, highlighting therapeutic potential in KRAS-driven PDAC (16).

1.3 Current Therapeutic Approaches and Limitations

1.3.1 Current Therapeutic Approaches

The standard therapeutic approaches for pancreatic cancer depend on the stage at diagnosis. For the minority of patients with localized, resectable tumors, surgical resection followed by adjuvant chemotherapy offers the best chance for long-term survival (17). However, even among those undergoing complete resection, recurrence rates remain high due to micrometastatic disease and resistance to systemic therapies. For patients with locally advanced or metastatic PDAC, systemic chemotherapy remains the mainstay of treatment. The combination regimen FOLFIRINOX (leucovorin, fluorouracil, irinotecan, and oxaliplatin) has demonstrated improved median overall survival compared to gemcitabine monotherapy in fit patients, although it is associated with significant toxicity (18). An alternative first-line option, gemcitabine combined with NPs albumin-bound paclitaxel (nab-paclitaxel), has also shown survival benefits in metastatic PDAC and is often used in patients with a lower performance status (19, 20).
In recent years, molecularly targeted therapies and immunotherapies have gained attention. For example, poly (ADP-ribose) polymerase (PARP) inhibitors are approved for patients with germline BRCA mutations; however, these mutations occur in only about 4–7% of pancreatic cancer cases, thus representing a limited patient subgroup (21, 22).

1.3.2 Treatment Limitations in PDAC

Despite modest progress, the prognosis for PDAC remains poor, largely due to biological and microenvironmental factors that render it refractory to both conventional and emerging treatments. PDAC is characterized by a dense desmoplastic stroma and hypovascular tumor core, which together impede drug delivery and facilitate immune evasion (23). The immunosuppressive tumor microenvironment is further reinforced by regulatory T cells, tumor-associated macrophages, and myeloid-derived suppressor cells, which suppress antitumor immune responses (24). As a result, immune checkpoint inhibitors—transformative in other cancers—have shown limited efficacy in PDAC (25).

To address these limitations, immune-stimulatory agents such as polyinosinic:polycytidylic acid (PolyIC), a synthetic analog of double-stranded RNA, have been proposed as adjuvants to reverse immune exclusion (26, 27). By activating Toll-like receptor 3 (TLR3) on dendritic cells and epithelial cells, PolyIC triggers type I interferon production and enhances antigen presentation, potentially transforming the tumor into an immunologically responsive environment (26, 28-30). Co-delivery of PolyIC with chemotherapeutics in NPs platforms offers a promising strategy to both induce tumor cell death and stimulate antitumor immunity.

In parallel, targeting KRAS G12D—the most common oncogenic driver in PDAC—remains challenging due to the structural and biochemical properties of the KRAS protein. KRAS binds GTP and GDP with very high affinity, complicating competitive inhibition at its active site (31). Additionally, its relatively smooth protein surface lacks distinct binding pockets, limiting stable interactions with small molecules. However, recent advances have led to promising KRAS-targeted inhibitors, including AMG 510 (sotorasib) and MRTX1133, which have shown encouraging results in preclinical studies and early-phase clinical trials (14, 16). Despite these advancements, targeting the G12D mutation specifically remains challenging, as it impairs intrinsic GTPase activity, leading to sustained activation of pathways such as MAPK and PI3K–AKT (32).

Rather than targeting the protein directly, an alternative strategy involves suppressing *KRAS* expression using small interfering RNA (siRNA). This approach enables sequence-specific degradation of mutant mRNA, reducing KRAS protein levels at the source (33). However, siRNA is inherently unstable in biological fluids, poorly taken up by cells, and prone to endosomal entrapment once internalized (34).

1.4 Combination Therapy for Pancreatic Cancer

While current chemotherapeutic regimens provide modest survival benefits in PDAC, their efficacy is ultimately limited by therapeutic resistance and immune evasion. Recent clinical studies have explored rationally designed combination therapies aimed at improving outcomes by targeting multiple tumor vulnerabilities simultaneously. For instance, the Chemo4METPANC phase II trial demonstrated that adding immunomodulatory agents to chemotherapy—specifically, combining gemcitabine and nab-paclitaxel with a PD-1 inhibitor (cemiplimab) and a CXCR4 antagonist (motixafortide)—achieved disease control in the majority of treated patients, including partial responses in over half the cohort. Similarly, the CANFOUR trial evaluated nadunolimab (anti-IL1RAP) alongside chemotherapy, showing encouraging median progression-free (7.1 months) and overall survival (13.2 months) in metastatic PDAC (35).

KRAS-based combination therapies also represent a promising area of research. Clinical studies have assessed combinations of chemotherapy with ERK1/2 inhibitors, such as Ulixertinib, which resulted in median overall survival of 12.23 months in metastatic PDAC patients (36). Additionally, early trials of KRAS G12D-targeted small molecules like RMC-9805 showed significant disease control (80%) and objective response rates (30%) in KRAS-mutant patients. RNA interference-based approaches, including siG12D-LODER™ implants and engineered exosomes carrying KRAS G12D siRNA, have demonstrated substantial preclinical efficacy and encouraging early clinical outcomes, including disease stabilization and partial responses. A Phase I/IIa study tested siG12D-LODER™ implants combined with gemcitabine in unresectable PDAC patients. Of 15 participants, 10 of 12 evaluable patients achieved disease stabilization, two had partial responses, with median overall survival of 15.1 months and 18-month survival rate of 38.5% (37).

These outcomes reflect a broader shift toward combination regimens that integrate cytotoxic and molecularly targeted mechanisms. Rather than replacing standard chemotherapy, such strategies

aim to build upon it—enhancing response rates, delaying resistance, and potentially sensitizing tumors to immunotherapy. Collectively, these findings support the continued development of combination platforms—particularly those capable of engaging both oncogenic drivers and the suppressive tumor microenvironment—as a necessary evolution in PDAC treatment.

1.5 Nanotechnology in Overcoming Drug Delivery Challenges

1.5.1 Advantages of Nanoparticle-based Drug Delivery Systems

To overcome these barriers, nanoparticles (NPs)–based systems have increasingly emerged as a promising approach in cancer therapy. NPs offer numerous advantages due to their unique physical and chemical properties, making them particularly suited to addressing challenges in cancer treatment such as targeted drug delivery, overcoming biological barriers, and minimizing systemic toxicity. The nanoscale size of these particles (typically 10–100 nm) enables preferential accumulation in tumor tissues through the enhanced permeability and retention (EPR) effect, which results from the hyper-permeable vasculature and impaired lymphatic drainage characteristic of solid. This passive targeting capability not only improves drug localization within tumors but also significantly reduces rapid renal clearance and nonspecific distribution, thus enhancing therapeutic efficacy while minimizing systemic adverse effects (38, 39).

Beyond passive targeting, NPs can be actively targeted through functionalization with specific ligands—such as antibodies, peptides, small molecules, or aptamers—that bind to receptors overexpressed on tumor cells or the tumor vasculature. This ligand-mediated active targeting further increases specificity, thereby reducing off-target effects and enhancing cellular uptake via receptor-mediated endocytosis (40, 41). For example, NPs conjugated with ligands targeting epidermal growth factor receptor (EGFR) or folate receptor have demonstrated significantly enhanced tumor-specific delivery in multiple cancer models, illustrating the potential of ligand-functionalization to markedly improve therapeutic precision (42).

Surface modification with biocompatible and hydrophilic polymers, most notably polyethylene glycol (PEG), has been extensively employed to enhance NPs circulation time and stability in biological fluids. This PEGylation process creates a hydrophilic corona around NPs, providing steric stabilization and reducing opsonization—the adsorption of serum proteins—which typically triggers rapid clearance by the mononuclear phagocyte system (43). Consequently, PEG-coated NPs exhibit prolonged circulation half-lives, enhancing the probability of tumor accumulation through passive and active targeting mechanisms (44).

NPs provide a versatile platform for simultaneously delivering multiple therapeutic agents, such as chemotherapeutics, nucleic acids, immunomodulators, and imaging agents. Co-delivery approaches target various tumor pathways, enhance therapeutic synergy, and help overcome drug resistance. For example, NPs carrying chemotherapeutics and siRNA effectively combat multidrug resistance and sensitize cancer cells to treatment (45, 46). Incorporating immunostimulatory agents with chemotherapy has also shown promise in activating immune

responses within immunologically "cold" tumors like pancreatic cancer (47). Collectively, these multifaceted capabilities highlight NPs not only as effective vehicles for targeted cancer therapy but also as critical tools in advancing personalized medicine by enabling more tailored and responsive therapeutic interventions.

1.5.2 Chitosan as a Biocompatible and Versatile Nanocarrier Material

Chitosan, a naturally occurring cationic polysaccharide derived from the deacetylation of chitin, has gained considerable attention as a nanocarrier in drug delivery systems. Its unique structural properties—including a high density of primary amine groups—enable strong electrostatic interactions with negatively charged biomolecules such as nucleic acids, making it particularly effective for siRNA delivery (48-50). In addition, chitosan is biodegradable, biocompatible, and exhibits low toxicity, which are critical features for clinical translation (51).

One of chitosan's most valuable features is its ability to form self-assembled NPs or polyplexes in aqueous conditions through ionic gelation or complexation (52). This allows for the facile encapsulation of therapeutic agents without the need for harsh solvents or high-energy processing. Its mucoadhesive properties also enhance its potential for mucosal and systemic administration by improving residence time and cellular uptake (53).

Beyond nucleic acid delivery, chitosan has demonstrated compatibility with small molecule chemotherapeutics, particularly hydrophobic drugs like PTX (54). Its structure allows for chemical conjugation or physical entrapment of drugs, enabling the co-delivery of multiple therapeutic agents within a single NPs system (55). This makes chitosan an attractive platform for developing combination therapies that integrate chemotherapy with gene-silencing strategies, which is especially relevant in resistant cancers such as PDAC.

1.6 Objective and Approach

1.6.1 Objective

To develop and optimize CP-PTX NPs as a platform approach for co-delivering PTX with either immunostimulatory PolyIC or KRAS-silencing siRNA, targeting critical vulnerabilities in pancreatic cancer cells. This modular dual-agent platform is designed to integrate chemotherapy with immunotherapy or genetic targeting, aiming to enhance therapeutic efficacy against PDAC.

1.6.2 Approach

CP-PTX-PolyIC Co-formulation and Evaluation

The first step of our approach involves the development and characterization of CP-PTX NPs co-loaded with PolyIC, a synthetic double-stranded RNA analog with immunostimulatory properties. This formulation—previously optimized and validated in multiple cancer models including pancreatic (Pan02) cells—demonstrated effective cellular uptake, robust cytotoxicity,

and enhanced dendritic cell activation. These studies established the CP-PTX-RNA platform as a proof-of-concept for combining chemotherapy and immunotherapy within a single NPs system.

CP-PTX-siRNA Co-formulation and Evaluation

Building on the knowledge from CP-PTX-PolyIC studies, the second step is to re-engineer the NPs preparation for gene silencing by incorporating small interfering RNA (siRNA) targeting KRAS G12D mutations. The system is first evaluated using luciferase siRNA in luciferase-expressing Pan02 cells to assess siRNA loading and gene knockdown efficiency. After optimization, KRAS siRNA is delivered to KRAS-mutant PDAC cells (PANC-1) to evaluate synergistic effects on cytotoxicity and gene silencing.

1.7 Scope and Significance

This thesis aims to significantly impact pancreatic cancer treatment by developing innovative NPs-based delivery systems targeting key therapeutic barriers. Specifically, with the successful development of chitosan NPs for the co-delivery of PTX and KRAS-targeting siRNA, the research holds potential to enhance therapeutic efficacy, address multidrug resistance, and inhibit critical genetic drivers in pancreatic cancer progression. These advancements could reshape current treatment paradigms, providing new opportunities for managing aggressive pancreatic cancers characterized by challenging tumor biology.

Beyond pancreatic cancer, this research contributes broadly to nanomedicine by demonstrating the utility of NPs in simultaneously overcoming multidrug resistance and genetic barriers prevalent across various cancers. The versatility of the developed NPs platform provides a modular approach, adaptable to different combinations of therapeutic agents and genetic targets, thereby fostering advancements in personalized and precision medicine strategies within oncology.

2. Material and methods

2.1. Materials

All chemicals were purchased from Sigma-Aldrich (St. Louis, MO, USA) unless otherwise stated. Chitosan powders were purchased from ChitoLytic Biotech Ltd. (Jiangsu, China) (MW ~3900, deacetylation rate 91.5%) and ChiBio Biotech Co., Ltd. (Qingdao, China) (MW < 3000, deacetylation rate ~98%). PTX was purchased from LC Laboratories (Woburn, MA, USA). Bovine serum albumin, wheat germ agglutinin–Alexa Fluor 555 conjugate, 8-well Nunc™ Lab-Tek™ II Chambered Coverglass, eBioscience™ Calcein AM Viability Dye (UltraPure Grade), and propidium iodide were purchased from ThermoFisher Scientific (Waltham, MA, USA). NucBlue DAPI reagent, Dulbecco's Modified Eagle Medium (DMEM), and RPMI 1640 cell culture medium were purchased from Invitrogen (Carlsbad, CA, USA). HyClone characterized fetal bovine serum (FBS) was purchased from GE Healthcare Life Sciences (Pittsburgh, PA,

USA). SpectraPOR7 1 kDa RC dialysis tubing was purchased from Repligen Corp (Waltham, MA, USA).

Pan02 and Pan02-Luciferase (Pan02-Luc) murine pancreatic cancer cells were obtained from the National Cancer Institute (NCI) Division of Cancer Treatment and Diagnosis Tumor Repository (Frederick, MD, USA). Human PANC-1 pancreatic cancer cells were purchased from the American Type Culture Collection (ATCC, Manassas, VA, USA). Recombinant murine GM-CSF was purchased from Peprotech (Cranbury, NJ, USA). The CellTiter-Glo® 3D cell viability assay kit was purchased from Promega (Madison, WI, USA). Fixation buffer, TruStain FcX™ PLUS (anti-mouse CD16/32) antibodies, PE anti-mouse CD11c, APC anti-mouse CD86, and FITC anti-mouse CD80 antibodies were purchased from BioLegend (San Diego, CA, USA). Luciferase-targeting siRNA (sense: 5'-CUUACGCUGAGUACUUCGAdTdT-3') and KRAS G12D-targeting siRNA (sense: 5'-GUUGGAGCUGAUGGCGUAGdTdT-3') were purchased from Dharmacon, Inc. (Lafayette, CO, USA).

For all experiments involving siRNA controls, siRNA was delivered using Lipofectamine™ 3000 (Thermo Fisher Scientific) according to the manufacturer's protocol. Briefly, siRNA was incubated with Lipofectamine 3000 reagent in Opti-MEM for 10–20 minutes at room temperature before being added to cells.

2.2. Synthesis of Paclitaxel-Carboxylic Acid (PTX-COOH)

PTX-COOH was prepared by modifying a previously established method (56). Briefly, PTX (50 mg) was reacted with succinic anhydride (11.8 mg) in 6 mL of chloroform containing 56.9 μL of pyridine. The solution was stirred at ambient temperature for 24 hours to allow complete derivatization. After the reaction, the solvent was removed by vacuum drying overnight. The resulting solid was collected and washed three times with deionized water using centrifugation (4000 ×g, 2 minutes) to remove unreacted reagents. The washed residue was redissolved in 2 mL of acetone and transferred to a 15 mL conical tube. Water was slowly added (~10 mL total) until the solution became visibly turbid, at which point the mixture was centrifuged at 1000 ×g for 10 minutes. The pellet was resuspended in 2 mL of deionized water and freeze-dried to yield purified PTX-COOH.

2.3. Conjugation of PTX-COOH to Chitosan-PEG

Chitosan-PEG (CP) was synthesized as described previously (57). For PTX conjugation, PTX-COOH (4.3mg) was activated by reacting with EDC (3.2 mg) and NHS (1.6 mg) in 0.5 mL of DMSO for 3 hours on a rocker. Separately, CP (20 mg) was dissolved in 0.8 mL of 0.1 M sodium bicarbonate buffer (pH 8.5), then diluted with 1.6 mL of DMSO. The activated PTX-COOH solution was gradually added to the CP solution under stirring and allowed to react overnight.

To reduce the DMSO concentration, 8 mL of deionized water was added dropwise to the mixture. The solution was then transferred into dialysis tubing (1 kDa MWCO, RC) and dialyzed

against 2 L of deionized water for 24 hours with changes at 1, 3, and 7 hours. After dialysis, the full content—including any precipitates—was subjected to bath sonication using a Fisher Sonic Dismembrator (Model 500) for 10 minutes at 40% amplitude (pulse mode: 10 s on, 5 s off). The mixture was centrifuged at 20,000 ×g for 10 minutes, and the supernatant containing CP-PTX was collected and stored at 4°C.

To fluorescently label the NPs, 2.7 mL of CP-PTX solution was mixed with 0.3 mL of 10× PBS (pH 7.4), and 10 µL of NHS-Cy5 (5 mg/mL in DMSO) was added. The reaction proceeded for 2 hours at room temperature with rocking. Excess dye was removed by 24-hour dialysis against deionized water using 1 kDa MWCO tubing, with three water changes. The concentration of CP-PTX and Cy5-labeled CP-PTX was determined by freeze-drying 10 mL of solution and weighing the dry mass.

2.4 Formulation of CP-PTX NPs

2.4.1 Nanoparticle Co-loading with PolyIC

PolyIC (MW 90-1,400) was first diluted in nuclease-free water to 1 mg/mL and then added to CP-PTX or Cy5-labeled CP-PTX at specified mass ratios. Bovine serum albumin (BSA), prepared as a 40 mg/mL stock solution in nuclease-free water, was added to reach a final concentration of 0.3 mg/mL to stabilize the nanocomplexes. All components were mixed in nuclease-free water and gently pipette-mixed to ensure uniform distribution.

2.4.2 Nanoparticle Co-loading with siRNA

For siRNA loading, siRNA stock solution (20 μM in RNase-free water) was mixed with CP-PTX NPs at predetermined mass ratios to form siRNA-loaded nanocomplexes. All components were mixed in nuclease-free water. Complexation was facilitated by water bath sonication at 60 kHz, using a pulsed cycle of 10 seconds on and 5 seconds off for a total of 5 minutes at 25 °C.

2.5 Physicochemical Characterizations

2.5.1 ^{1}H Nuclear Magnetic Resonance (^{1}H NMR) Characterization

NMR spectra were acquired using a Bruker AVANCE III 500 MHz spectrometer operating at a ^{1}H frequency of 499.65 MHz. CP and CP-PTX samples were dissolved in D_2O, while PTX was measured in DMSO-d_6. Acquisition parameters included: 96 scans (NS), acquisition time (AQ) of 2.34 seconds, and time domain (TD) of 32,678 points.

To quantify PTX content in the conjugate, a dried sample was redissolved in 0.9 mL of D_2O and mixed with 0.1 mL of TSP (3-(Trimethylsilyl) propionic-2,2,3,3-d_4 acid sodium salt) solution at 17.2 mg/mL. Peak integrations at δ = 7.75 ppm (PTX, 2H) and δ = 0.00 ppm (TSP, 9H) were used to calculate PTX content via the equation (58):

$$m_{D=}\frac{m_{IS}P_{IS}I_{D}M_{D}}{M_{IS}P_{D}I_{IS}}$$

Where:

- m_D: mass of PTX
- m_{IS}: mass of internal standard (TSP)
- P_D, P_{IS}: number of protons corresponding to the drug and internal standard peaks
- I_D, I_{IS}: integrated peak areas
- M_D, M_{IS}: molecular weights of PTX and TSP, respectively

2.5.2 Dynamic Light Scattering

Hydrodynamic size, polydispersity index (PDI), zeta potential, and conductivity were measured using a Zetasizer Nano-ZS (Malvern Instruments, UK). Measurements were performed at room temperature in both deionized water and HEPES buffer (pH 6.8).

2.6 Cell Culture

Pan02 and Pan02-Luc cells were maintained in RPMI medium supplemented with 10% fetal bovine serum (FBS) and 1% penicillin–streptomycin. PANC-1 cells were cultured in DMEM with 10% FBS and 1× penicillin–streptomycin. All cell lines were incubated at 37 °C in a humidified incubator with 5% CO_2.

2.7 Cellular Co-delivery of CP-PTX-PolyIC NPs

2.7.1 Cell Uptake of CP-PTX-PolyIC NPs

To evaluate CP-PTX-PolyIC NPs uptake, Pan02 cells were seeded at 8,000 cells per well in an 8-well chambered coverglass and incubated for 24 hours. Pan02 is a murine pancreatic ductal adenocarcinoma cell line commonly used in immunocompetent mouse models due to its aggressive growth and tumor microenvironment characteristics, making it a suitable *in vitro* model for NPs uptake and drug delivery studies. Cells were then treated with 100 µg/mL of Cy5-labeled CP-PTX-PolyIC for 2 hours at 37 °C. After treatment, cells were fixed with 4% paraformaldehyde, and cell membranes were stained with wheat germ agglutinin–Alexa Fluor 555. Nuclei were counterstained with DAPI. Cellular uptake and intracellular distribution of the NPs were assessed using confocal laser scanning microscopy.

2.7.2 Cytotoxicity Assay of CP-PTX-PolyIC NPs

Pan02 cells were seeded at 4,000 cells per well in 96-well plates and incubated for 24 hours before treatment. Cells were then exposed to various formulations—PolyIC, CP, PTX, CP-PTX, or CP-PTX-PolyIC—for 48 hours. All doses were normalized to the component amounts present in the CP-PTX-PolyIC formulation containing 2 µM PTX (PolyIC = 425 µg/mL). The PTX concentrations in CP-PTX and CP-PTX-PolyIC were quantified using NMR analysis. Following

treatment, brightfield images were acquired using a Nikon TE300 inverted fluorescence microscope. Cell viability was assessed by measuring intracellular ATP using the CellTiter-Glo® 3D cell viability assay kit, with values normalized to untreated control cells (set as 100%). Additionally, live/dead staining was performed on both untreated and PTX-treated Pan02 cells using calcein AM and propidium iodide, following the manufacturer's protocol. Live cell intensities were quantified using ImageJ software (version 1.53t).

2.8 Cellular Co-delivery of CP-PTX-Luc siRNA NPs

2.8.1 Luciferase Knockdown of CP-PTX-Luc siRNA NPs

The Pan02-Luc cell line, a luciferase-expressing variant of the murine pancreatic cancer line Pan02, was selected to enable real-time, quantitative assessment of gene silencing via luminescence-based imaging. This model is well-suited for evaluating siRNA-mediated knockdown in an immune-relevant pancreatic cancer context. Luciferase Knockdown of Luc siRNA NPs Pan02-Luc cells were seeded at 15,000 cells per well in a 96-well plate and incubated for 24 hours. Cells were then treated with CP-PTX–Luc siRNA NPs (26 µg/mL) or free Luc siRNA transfected using Lipofectamine™ RNAiMAX (Thermo Fisher Scientific) according to the manufacturer's protocol. Following a 24-hour incubation, luciferase activity was assessed using both a luminescence plate reader and a Xenogen IVIS 200 imaging system (PerkinElmer, Inc., Waltham, MA, USA). The IVIS imaging parameters were set as follows: Field of view, 10; excitation filter, closed; emission filter, open; exposure time, 60 s; binning factor, 4; f/stop, 1. D-luciferin (Waltham, MA, USA) was added directly to each well at a final concentration of 3 mg/mL. For plate reader measurements, luminescence was recorded after a 5-minute incubation using a microplate luminometer. For IVIS imaging, bioluminescent images were acquired immediately after luciferin addition with the following settings: 1-minute exposure time, medium binning, f/stop 1, emission filter set to 'open', and field of view set to C. Subject height was set to 0.5 cm, and focus was adjusted accordingly. Total photon flux was quantified using Living Image software and normalized to untreated controls to evaluate luciferase knockdown efficiency.

2.8.2 Cytotoxicity of CP-PTX-Luc siRNA NPs

Pan02-Luc cells were seeded at 15,000 cells per well in a 96-well plate and incubated for 24 hours. Cells were then treated with 26 µg/mL of CP-PTX–Luc siRNA NPs and incubated for 24 hours at 37 °C. Following treatment, cell viability was assessed using the Alamar Blue assay according to the manufacturer’s instructions. Fluorescence intensity was measured using a plate reader to evaluate metabolic activity and infer siRNA-induced cytotoxic effects.

2.9 Cytotoxicity of PTX-KRAS G12D siRNA NPs

The PANC-1 human pancreatic cancer cell line was chosen due to its well-characterized KRAS G12D mutation, which makes it a relevant *in vitro* model for evaluating the therapeutic effects of KRAS-targeting siRNA in human PDAC (59). A 72-hour incubation period was used—longer

than in other assays—to allow sufficient time for siRNA-mediated gene silencing to take effect and for downstream cytotoxic responses to manifest. PANC-1 cells were seeded at 10,000 cells per well in a 96-well plate and allowed to attach for 24 hours. Cells were then treated with 26 μg/mL of CP-PTX–KRAS G12D siRNA NPs and incubated for 72 hours at 37 °C. After treatment, Alamar Blue reagent was added to each well, and fluorescence was measured after incubation to quantify cell viability and assess the impact of KRAS knockdown.

2.10 Statistical Analysis

All data are presented as mean ± standard error of the mean (SEM), unless otherwise indicated. Statistical significance was assessed using one-way analysis of variance (ANOVA). For comparisons between two groups, an unpaired two-tailed Student's t-test was used. A p-value less than 0.05 was considered statistically significant. Significance levels are indicated as follows: $P < 0.05$ (*), $P < 0.01$ (**), $P < 0.001$ (***), and $P < 0.0001$ (****).

3. Results and Discussion

3.1 Design of the CP-PTX NPs Platform

We designed a multifunctional NPs system based on CP-PTX for co-delivery of PTX and polyinosinic-polycytidylic acid (PolyIC), a synthetic double-stranded RNA analog known to activate dendritic cells via Toll-like receptor 3 (TLR3), thereby inducing antitumor immune responses. The system was constructed by first modifying PTX with succinic anhydride to form carboxylated PTX (PTX-COOH), which was then covalently conjugated to a chitosan-polyethylene glycol (CP) carrier via EDC/NHS chemistry. The resulting CP-PTX conjugate, bearing primary amines from chitosan, exhibited a net positive charge and allowed for electrostatic complexation with negatively charged PolyIC, forming CP-PTX-PolyIC NPs (**Figure 1a**). This covalent conjugation strategy contrasts with many NPs systems reported in the literature, which commonly rely on passive physical encapsulation of PTX into lipid or polymeric carriers. Such approaches often suffer from burst release and limited drug retention, whereas our design enables pH-sensitive intracellular release through hydrolysable amide bonds, improving control over drug availability in the tumor microenvironment (Wang et al., 2024).

Given the structural and electrostatic similarity between PolyIC and small interfering RNA (siRNA), we adapted this platform for RNA interference-based therapeutics. PolyIC served as a model nucleic acid for initial optimization of NPs formation, charge balance, and stability. After establishing optimal parameters with PolyIC, we transitioned to luciferase siRNA to evaluate gene silencing performance *in vitro*. This step provided a tractable system to refine formulation and transfection conditions.

Finally, the optimized platform was applied to deliver KRAS G12D-targeting siRNA, enabling selective post-transcriptional silencing of oncogenic KRAS in pancreatic cancer models. This modular evolution—from immunostimulatory PolyIC to gene-silencing siRNA—demonstrates the

flexibility of the CP-PTX delivery system and its potential for both immune modulation and targeted gene knockdown applications. In contrast to several published KRAS-targeting NPs platforms, which utilize peptide-based or peptide-nucleic acid conjugates with limited adaptability or involve complex formulations prone to instability, our CP-based system provides a simplified yet tunable scaffold for multiplexed therapeutic delivery.

Figure 1b illustrates the potential interactions of the designed NPs within the tumor microenvironment. Upon systemic administration and cellular uptake by tumor cells, the acidic conditions in endosomes or lysosomes promote the hydrolysis of the amide bond linking PTX to the carrier, triggering the intracellular release of active PTX. PTX exerts its cytotoxic effect by stabilizing microtubules and inhibiting mitotic spindle disassembly, resulting in mitotic arrest and apoptosis of rapidly dividing tumor cells.

Simultaneously, the KRAS G12D-targeting siRNA is released from the NPs matrix and incorporated into the RNA-induced silencing complex (RISC) in the cytoplasm. Guided by sequence complementarity, the siRNA-RISC complex selectively binds and degrades KRAS G12D mutant mRNA, leading to suppression of downstream oncogenic signaling pathways such as MAPK and PI3K/AKT. This post-transcriptional silencing inhibits tumor cell proliferation and survival and can reduce intrinsic resistance mechanisms to chemotherapeutics.

Importantly, these two agents function synergistically: PTX disrupts the mitotic process to induce apoptosis, while KRAS G12D siRNA targets the oncogenic signaling pathways that often drive chemoresistance. By downregulating KRAS activity, siRNA sensitizes tumor cells to PTX-induced mitotic stress, enhancing apoptosis even at lower PTX concentrations. This dual targeting—of both the cell cycle and survival pathways—results in a more comprehensive antitumor effect and may overcome resistance associated with single-agent therapies. Overall, our CP-PTX-siRNA platform integrates controlled chemotherapeutic release and targeted gene silencing in a single, biocompatible construct, distinguishing it from conventional systems and highlighting its potential for translational applications in combination nanomedicine.

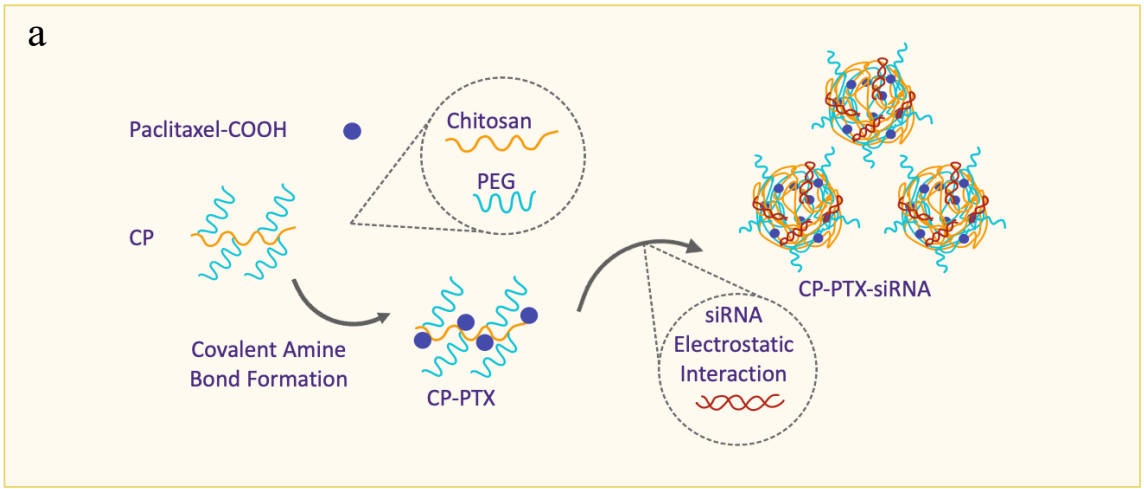

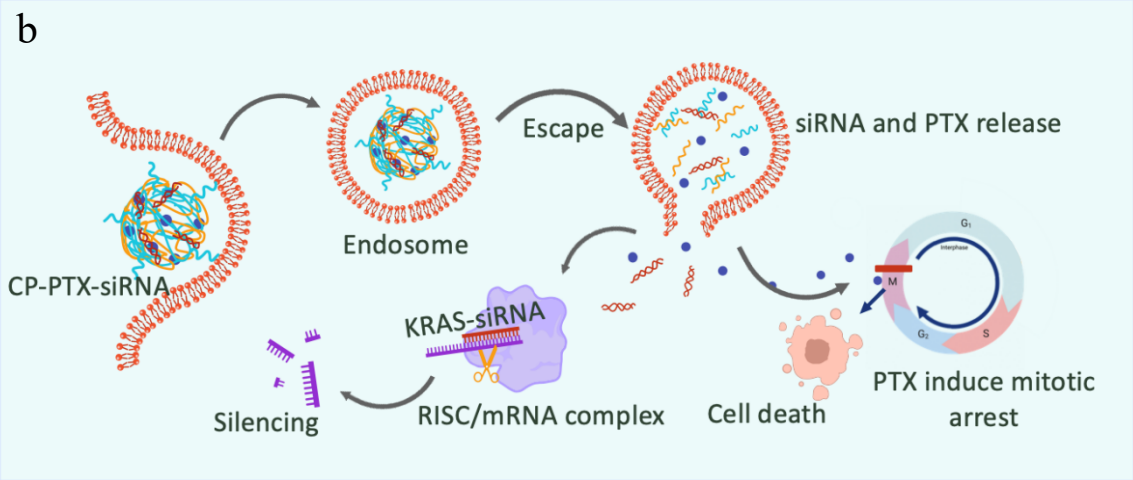

Figure 1. CP-PTX-siRNA NPs that co-delivers PTX and siRNA to cancer cells for combined chemo-gene therapy. (**a**) Schematic illustration of NPs synthesis. PTX was covalently conjugated to the CP polymer, composed of chitosan and polyethylene glycol (PEG), to form CP-PTX. The resulting CP-PTX was then complexed with siRNA via sonication to generate the final CP-PTX-siRNA NPs. (**b**) Illustrates the mechanism of action of CP-PTX-siRNA NPs. The NPs are designed to deliver both PTX and KRAS-targeting siRNA into cancer cells. Upon cellular uptake, the NPs are internalized into endosomes. After escaping the endosomes, the NPs release siRNA and PTX into the cytoplasm. The released KRAS-siRNA forms a complex with the RISC/mRNA complex, leading to the silencing of the KRAS gene. Meanwhile, PTX induces mitotic arrest in the M phase of the cell cycle, preventing cell division. The combined effects of KRAS silencing and PTX-induced mitotic arrest ultimately result in cell death, demonstrating the dual therapeutic action of the CP-PTX-siRNA NPs system.

3.2 Synthesis and Structural Validation of CP-PTX

We synthesized CP-PTX NPs by covalently attaching carboxylated PTX to a chitosan-polyethylene glycol (CP) carrier, resulting in a water-soluble and stable polymer-drug complex (**Figure 2a**). To enhance aqueous solubility and accommodate hydrophobic drug loading, ultralow molecular weight chitosan (MW ~3.9 kDa) was first functionalized with PEG. PTX was modified using succinic anhydride under basic conditions to form 2′-succinyl PTX (PTX-COOH), which allowed for pH-responsive release in the acidic tumor microenvironment. The conjugation of PTX-COOH to primary amine groups on CP was achieved via carbodiimide chemistry using EDC and NHS in a sodium bicarbonate/DMSO buffer (pH 8.5), forming stable amide bonds.

Successful formation of the CP-PTX conjugate was verified through nuclear magnetic resonance (NMR) spectroscopy (**Figure 2b**). The characteristic resonance signals from chitosan and PEG appeared at 3.5–4 ppm, while aromatic protons from the PTX moiety were evident between 7–8.2 ppm—signals that were absent in the CP control, confirming drug attachment. In prior work using this same chemistry, formation of the amide linkage between PTX and CP was also validated by

Fourier transform infrared spectroscopy (FTIR). Based on NMR quantification, the drug loading efficiency reached approximately 3.21 wt%.

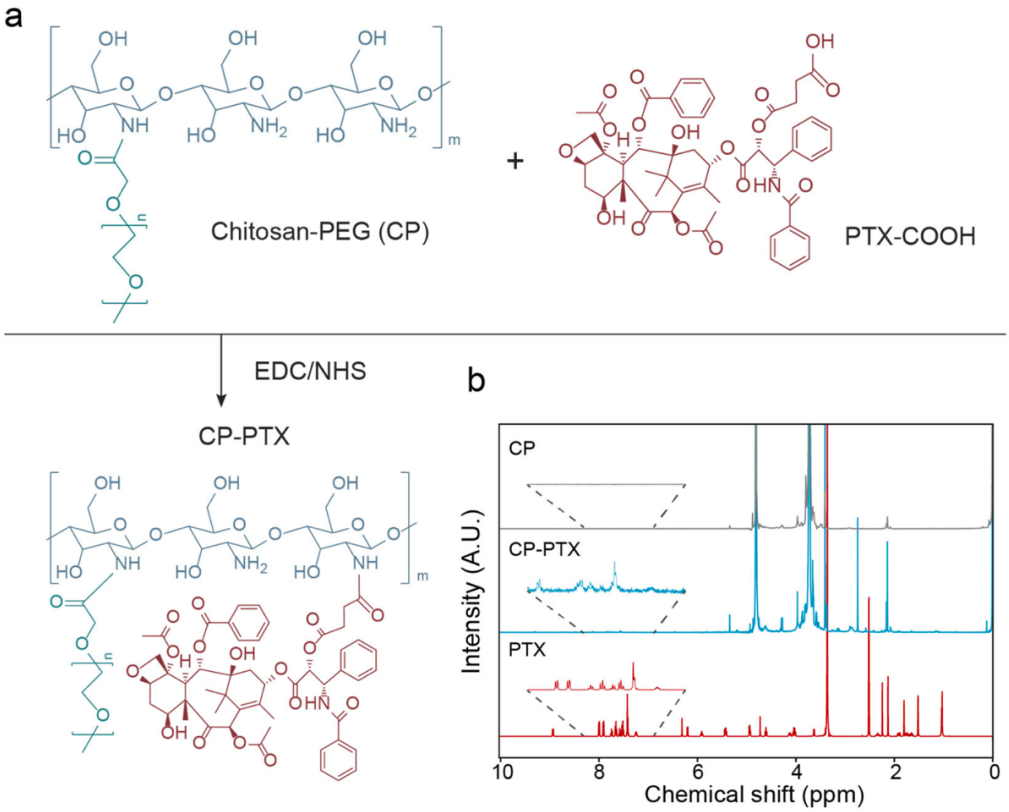

Figure 2. Synthesis and characterization of CP-PTX. (**a**) Schematic illustration of the chemical conjugation of carboxylated PTX (PTX-COOH) to the CP polymer using EDC/NHS-mediated coupling. (**b**) Representative ^{1}H NMR spectra of CP, CP-PTX, and free PTX confirming successful conjugation. Reproduced from Huang et al., *Pharmaceutics* 2024, *16*, 1246, under the terms of the Creative Commons Attribution (CC BY 4.0) license (60).

3.3 Physiochemical Properties of CP-PTX-PolyIC NPs

The physicochemical characteristics of CP-PTX-PolyIC NPs were further investigated to assess optimal nucleic acid loading. Negatively charged PolyIC was electrostatically associated with the positively charged CP-PTX polymer. To determine the optimal loading conditions, we measured the zeta potential of CP-PTX-PolyIC complexes prepared at different CP-PTX:PolyIC mass ratios (**Figure 3a**). The zeta potential of CP-PTX alone was measured at +14.3 mV. As increasing amounts of PolyIC were added, the zeta potential progressively decreased—dropping to +11.6 mV, +7.8 mV, and +4.1 mV at mass ratios of 46:1, 18:1, and 11:1, respectively—indicating successful loading of PolyIC. When PolyIC was added in excess, the surface charge reversed, becoming negative, with a zeta potential reaching −18.4 mV at a 6:1 mass ratio.

To support further stabilization via interactions with serum proteins such as albumin (which carries a net negative charge at physiological pH), a moderately positive NPs surface was preferred. As such, we selected the 11:1 CP-PTX:PolyIC ratio as the optimal formulation, striking a balance between effective PolyIC loading and maintaining a positive surface charge. At this ratio, the formulation corresponded to a PTX:PolyIC mass ratio of 1:14 and served as a proof-of-concept for the co-delivery platform. The relative drug loading ratio can be modified for future therapeutic applications. The selected intermediate CP-PTX-PolyIC formulation was subsequently incubated with albumin, forming a stabilized NPs system for downstream experiments.

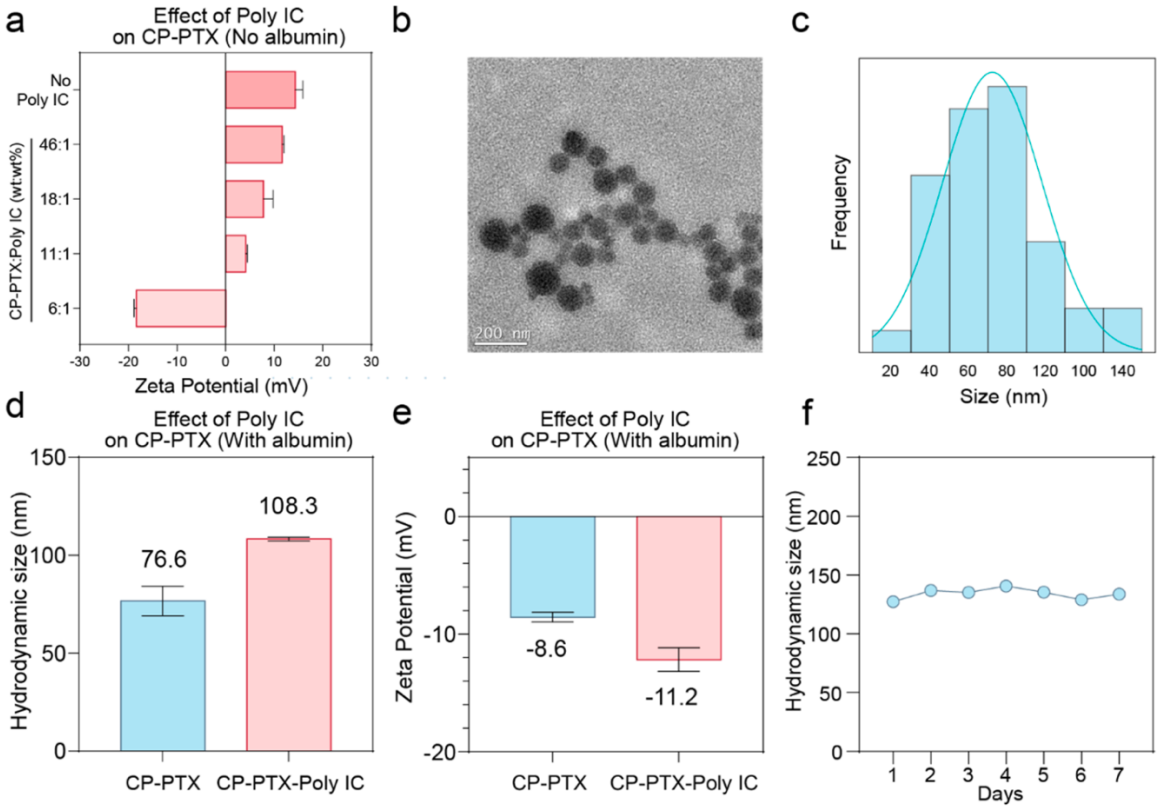

Figure 3. Characterization of CP-PTX-PolyIC NPs. (**a**) Zeta potential measurements of CP-PTX alone (intermediate (1) in Figure 1a) and CP-PTX-PolyIC complexes (intermediate (2)) prepared at various CP-PTX:PolyIC weight ratios (46:1, 18:1, 11:1, 6:1), assessed at room temperature. (**b**) Transmission electron microscopy (TEM) images of the final CP-PTX-PolyIC NPs. Scale bar: 200 nm. (**c**) Particle size distribution of CP-PTX-PolyIC NPs obtained from TEM image analysis. (**d**) Hydrodynamic diameter and (**e**) Zeta potential of albumin-stabilized CP-PTX and CP-PTX-PolyIC NPs (step (3) in Figure 1a), measured in water at pH ~7 and room temperature. (**f**) Hydrodynamic size stability of CP-PTX-PolyIC NPs monitored at 37°C in water over a period of 7 days. Reproduced from Huang et al., *Pharmaceutics* 2024**,** *16*, 1246, under the terms of the Creative Commons Attribution (CC BY 4.0) license (60).

3.4 Physiochemical Properties of CP-PTX-siRNA NPs

The physicochemical characteristics of the CP-PTX-siRNA NPs were analyzed to determine the optimal formulation for stability and delivery. KRAS G12D-targeting siRNA, which carries a strong negative charge, was complexed with cationic CP-PTX via electrostatic interactions. We evaluated various CP-PTX:siRNA mass ratios to assess their impact on NPs size and surface charge (**Figure 4**). At a 1:0 (no siRNA) ratio, particles exhibited a z-average size of 178.18 nm and a zeta potential of +3.44 mV. As the siRNA content increased, both the particle size and surface charge decreased, reflecting effective siRNA loading.

At a 1:0.2 ratio, the z-average decreased significantly to 56.83 nm, and the zeta potential shifted to −6.43 mV. The most compact and stable formulation was observed at a 1:0.1 mass ratio, with a z-average of 26.47 nm and a zeta potential of −9.76 mV. These values remained consistent after 24 hours (27.9 nm and −6.05 mV, respectively), indicating good colloidal stability over time. This formulation was selected as optimal due to its minimal size and stable, moderately negative surface charge, ideal for cellular uptake and circulation

Formulations with lower siRNA ratios, such as 1:0.05, produced slightly larger particles (~34.25 nm) with weaker negative surface charges (−2.07 mV), while formulations with higher siRNA content resulted in greater size variability or instability.

Overall, the 1:0.1 CP-PTX:siRNA mass ratio was identified as the most effective for dual-agent delivery, offering efficient siRNA loading, compact size, and suitable surface charge for *in vivo* application.

NPs size plays a critical role in determining circulation time, biodistribution, and tumor penetration. Particles larger than 200 nm are prone to rapid clearance by the mononuclear phagocyte system due to complement activation, while particles smaller than 10 nm are rapidly filtered by the kidneys (61). Thus, maintaining an intermediate size range is essential for achieving prolonged systemic circulation and effective tumor accumulation.

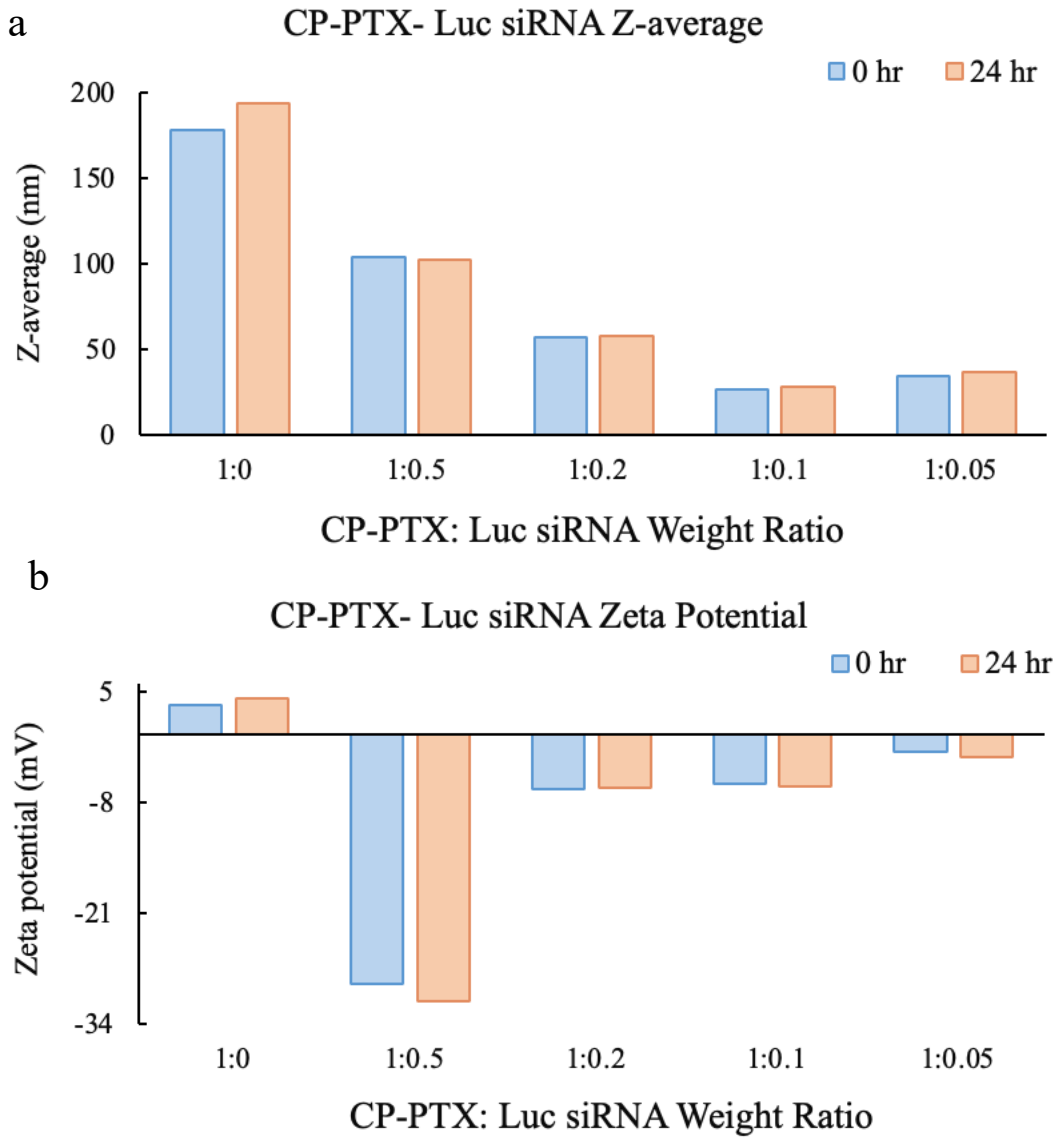

Figure 4. Characterization of CP-PTX-siRNA NPs with various CP-PTX: siRNA weight Ratios. Samples were measured immediately after formulation and after 24 hours. The data illustrate how the CP-PTX to Luc siRNA weight ratio influences NPs (**a**) and surface charge stability (**b**) over time.

3.5 Cellular Co-delivery of CP-PTX-PolyIC NPs

3.5.1 Cell Uptake of CP-PTX-PolyIC NPs

To evaluate intracellular delivery efficiency, cellular uptake of CP-PTX-PolyIC NPs was assessed in Pan02, a widely used murine pancreatic adenocarcinoma cell line that reliably models key features of human PDAC, including aggressive tumor growth, dense stroma formation, and immunosuppressive characteristics (62). Cy5-labeled CP-PTX was complexed with PolyIC and albumin to form fluorescently traceable NPs. Pan02 cells were incubated with the labeled CP-

PTX-PolyIC for 2 hours, after which nuclei were stained with DAPI (blue) and cell membranes with WGA-AF555 (green). Confocal microscopy imaging revealed clear internalization of Cy5-labeled NPs (red) within the cytoplasm, indicating efficient uptake.

These results confirm that CP-PTX-PolyIC NPs effectively penetrate Pan02 cell membranes and localize intracellularly, supporting their potential for delivering chemotherapeutic and immunomodulatory agents directly into pancreatic cancer cells **(Figure 5**).

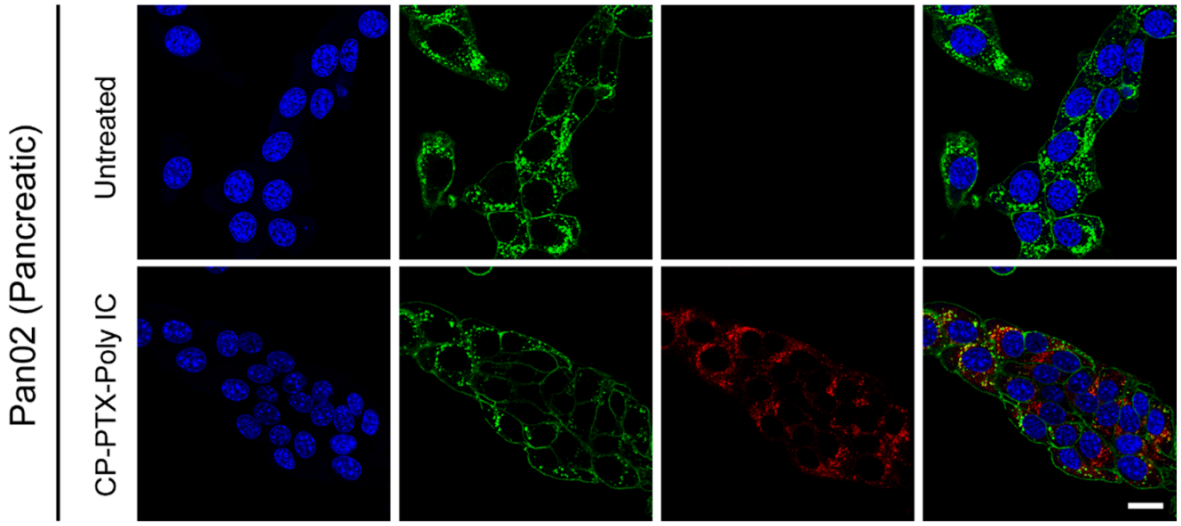

Figure 5. Cellular uptake of CP-PTX-PolyIC NPs in Pan02 cells. Confocal microscopy images of Pan02 cells incubated with Cy5-labeled CP-PTX-PolyIC for 2 hours. Untreated cells were used as a reference. Nuclei were stained with DAPI (blue), cell membranes with WGA-AF555 (green), and the red signal represents CP-PTX-PolyIC NPs. Scale bar: 20 µm. Reproduced from Huang et al., *Pharmaceutics* 2024**,** *16*, 1246, under the terms of the Creative Commons Attribution (CC BY 4.0) license (60).

3.5.2 Cytotoxicity Assay of CP-PTX-PolyIC NPs

The cancer-killing effect of CP-PTX-PolyIC NPs was evaluated in Pan02. Cells were treated with various formulations—PolyIC, CP, PTX, CP-PTX, and CP-PTX-PolyIC—at component concentrations equivalent to 2 µM PTX and incubated for 48 hours (**Figure 6**).

Brightfield imaging revealed that PolyIC and CP treatments had minimal impact on cell morphology and density compared to untreated controls. In contrast, PTX-containing formulations significantly reduced cell number. Notably, Pan02 cells treated with CP-PTX-PolyIC showed not only apoptosis but also cell enlargement, consistent with PTX's mechanism of action, which involves binding to the β-tubulin subunit of microtubules and disrupting mitotic spindle formation. This disruption leads to mitotic arrest and subsequent cell death.

To quantitatively assess viability, intracellular ATP levels were measured using the CellTiter-Glo® 3D cell viability assay. The ATP level of untreated cells was set to 100%. PolyIC and CP showed minimal cytotoxicity, while PTX, CP-PTX, and CP-PTX-PolyIC demonstrated significant reductions in ATP levels. In Pan02 cells, the relative ATP levels were as follows: 51.8 for PTX, 66.2 for CP-PTX, and 55.2 for CP-PTX-PolyIC.

To validate ATP-based viability results, live/dead staining was conducted. The live cell fluorescence intensity in CP-PTX-PolyIC-treated Pan02 cells was lower than the corresponding ATP levels, suggesting that ATP assays may slightly overestimate viability due to residual ATP in dead or dying cells.

These findings indicate that CP-PTX-PolyIC NPs exert potent cytotoxic effects on pancreatic cancer cells, driven primarily by the chemotherapeutic action of PTX, with potential enhancement through immune stimulation by PolyIC.

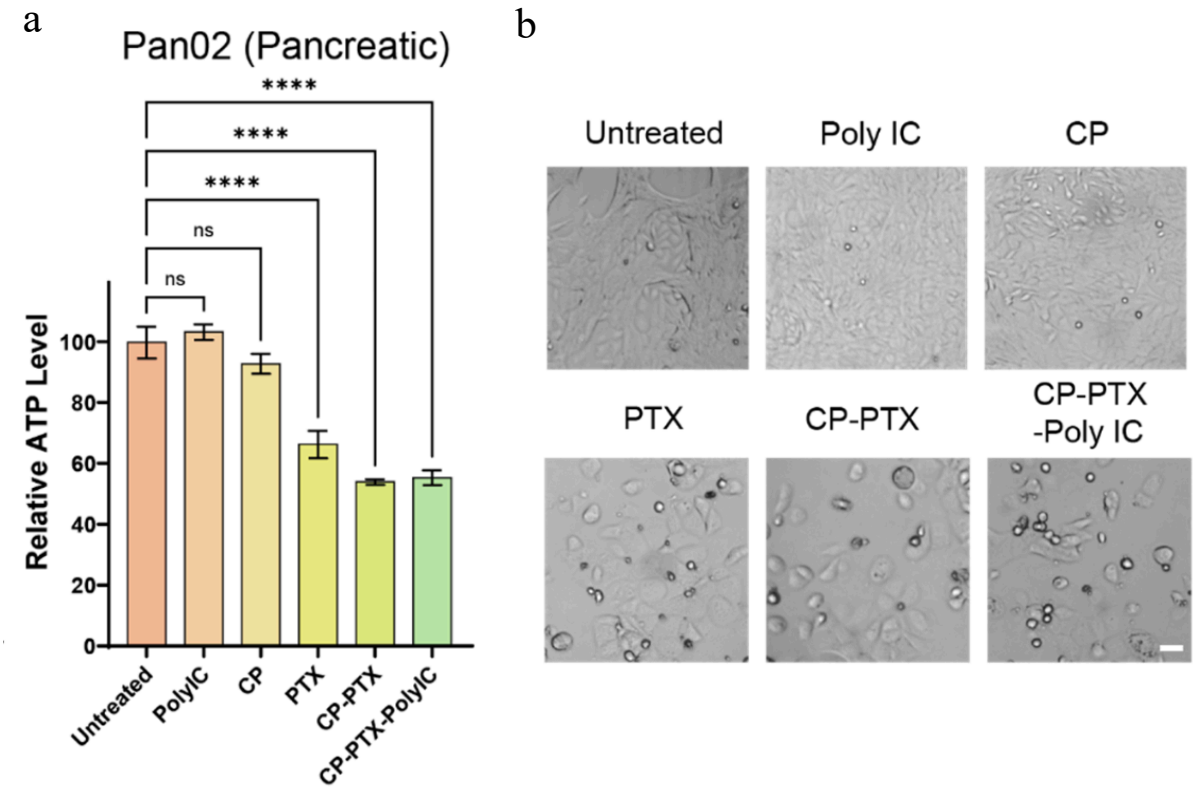

Figure 6. Cancer-killing effect of CP-PTX-PolyIC in Pan02 cells. (**a**)Relative ATP levels of Pan02 cells treated with PolyIC, CP, PTX, CP-PTX, and CP-PTX-PolyIC for 48 hours and (**b**) Brightfield images. The dose of each treatment was equivalent to the corresponding component amounts in CP-PTX-PolyIC at 2 µM PTX (PolyIC = 425 µg/mL). Scale bar: 50 µm. *$p < 0.05$, ****$p < 0.0001$, ns = not significant. Reproduced from Huang et al., *Pharmaceutics* 2024**,** *16*, 1246, under the terms of the Creative Commons Attribution (CC BY 4.0) license (60).

3.6 Cellular Co-delivery of CP-PTX-Luc siRNA NPs

3.6.1 Luciferase Knockdown by CP-PTX-Luc siRNA NPs

To evaluate the gene silencing efficiency of CP-mediated siRNA delivery, we measured luciferase expression in Pan02-Luc cells following treatment with various formulations containing luciferase siRNA. Luciferase activity was quantified 24 hours post-transfection and normalized to the untreated control group.

As shown in **Figure 7**, CP alone had minimal effect on luciferase expression (97% ± 10.0%), while Lipo-siRNA reduced expression to 22% ± 11.0%, serving as a positive control for knockdown efficiency. CP-siRNA achieved 52% ± 10.4% expression, confirming its ability to deliver functional siRNA. CP-PTX-siRNA resulted in 43% ± 9.8% luciferase activity, indicating that PTX conjugation did not hinder siRNA delivery.

Notably, CP-PTX-siRNA treatment also reduced luciferase expression to 43%, showing that the presence of conjugated PTX did not interfere with siRNA delivery or RISC loading. This dual-function NPs retained gene silencing activity while offering additional chemotherapeutic effects, as shown in the parallel viability assays. PTX and CP-PTX treatments without siRNA had no substantial effect on luciferase expression (58%), indicating that observed knockdown was siRNA-specific rather than a result of cytotoxic suppression of transcription.

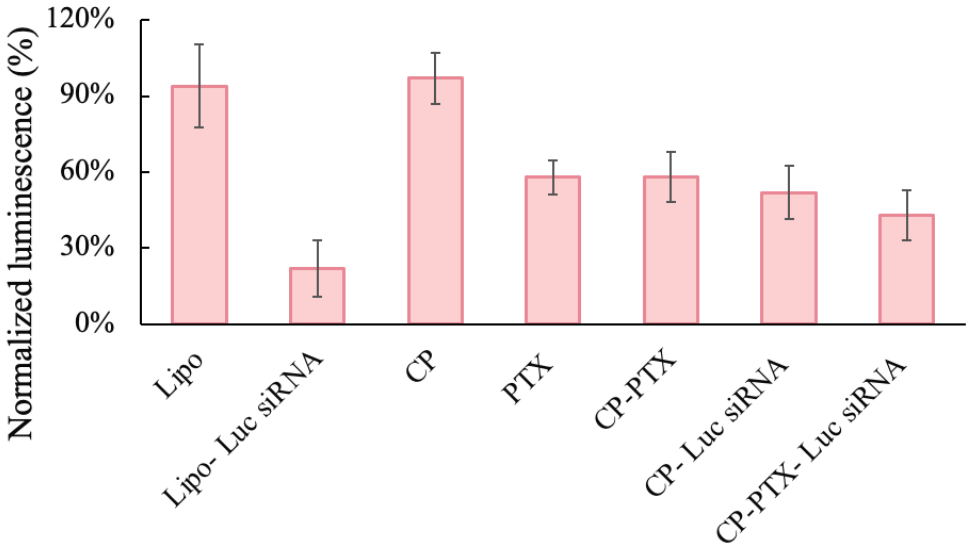

Figure 7. Luciferase RNAi of Pan02-Luc Cells after treatments. Pan02-Luc cells were seeded in a 96-well plate (1.5×10^4 cells/well) and cultured for 24 hours before treatment. Cells were treated with Lipo-siRNA, CP-siRNA, PTX, CP-PTX, CP-PTX-siRNA, or vehicle controls (Lipo and CP) for 24 hours. Luciferase siRNA concentration was fixed at 200 nM, and PTX concentration was fixed at 2.55 μM.

3.6.2 Cytotoxicity of CP-PTX-Luc siRNA NPs

To evaluate the therapeutic potential of the CP-PTX-siRNA NPs system, we conducted a cell viability assay using the luciferase-expressing murine pancreatic cancer cell line Pan02-Luc. Cells were treated for 24 hours with various formulations containing PTX, CP, and/or luciferase siRNA. Viability was quantified relative to untreated control cells.

As shown in **Figure 8**, CP alone demonstrated negligible cytotoxicity, maintaining cell viability at 95% ± 8.9%, consistent with its known biocompatibility. Free PTX significantly reduced viability to 50% ± 12.4%, while CP-PTX NPs exhibited a comparable reduction at 47% ± 13.3%, confirming that PTX remained active after conjugation. Lipofectamine-siRNA (Lipo-siRNA), used as a control siRNA formulation, resulted in a modest decrease in cell viability to 70% ± 8.8%, likely due to transfection-associated cytotoxicity. Similarly, CP-siRNA treatment resulted in 72% ± 9.7% viability, reflecting mild delivery-related stress rather than direct gene knockdown toxicity, as luciferase is a non-essential reporter gene.

Importantly, the combined delivery of PTX and siRNA in CP-PTX-siRNA NPs led to the most pronounced reduction in cell viability, down to 43% ± 23.6%. This enhanced cytotoxicity indicates a potential combinatorial effect, arising either from improved cellular internalization, synergistic intracellular stress, or cumulative delivery-associated cytotoxicity. However, the higher variability observed in the CP-PTX-siRNA group (±23.6%) suggests heterogeneity in NPs uptake or intracellular drug and siRNA release dynamics.

Collectively, these results demonstrate the capability of the CP-PTX-siRNA system to co-deliver PTX and siRNA effectively, highlighting its potential utility as a multifunctional therapeutic platform for KRAS-driven pancreatic cancers.

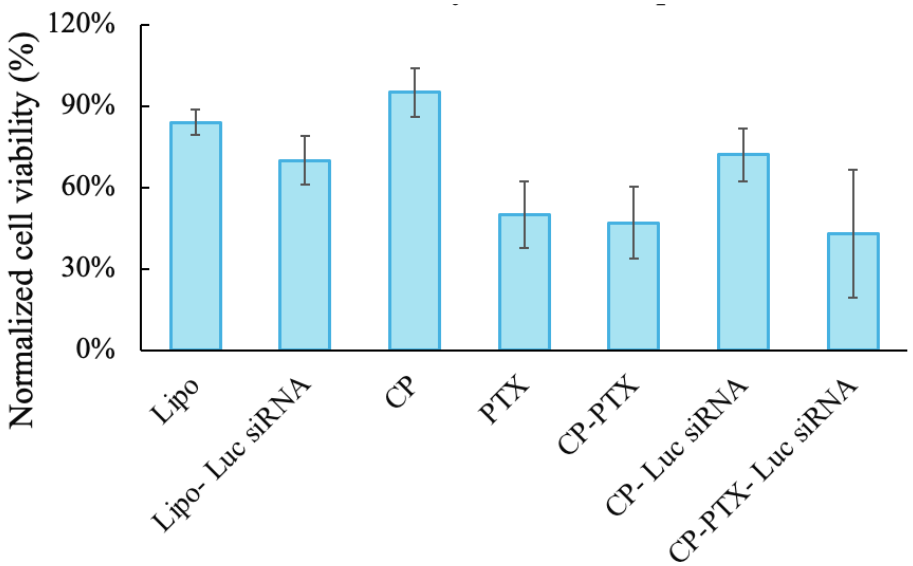

Figure 8. Luciferase RNAi and cell viability of Pan02-Luc Cells after treatment. Pan02-Luc cells were seeded on a 96-well plate (1.5×10^4 cells/well) and cultured for 24 hours before treatment. Cells were treated with Lipo-siRNA, CP-siRNA, PTX, CP-PTX, CP-PTX-siRNA, or vehicle controls (Lipo and CP) for 24 hours. Luciferase siRNA concentration was fixed at 200 nM, and PTX concentration was fixed at 2.55 μM.

3.7 Cytotoxicity of CP-PTX-KRAS G12D siRNA NPs

To evaluate potential therapeutic synergy of CP-PTX-KRAS siRNA NPs, we treated PANC-1 cells with PTX, KRAS G12D-targeting siRNA (delivered by Lipofectamine), or their combination in both free and NPs-conjugated forms at varying concentrations. Cell viability was assessed after 72 hours of treatment, normalized to untreated controls (100% viability).

As shown in **Figure 9**, single-agent treatments exhibited moderate dose-dependent cytotoxicity. Free PTX at concentrations of 50 nM and 100 nM resulted in cell viabilities of 78% (±13.4%) and 63% (±14.1%), respectively. Increasing PTX concentration to 200 nM slightly decreased viability further, to 61% (±11.3%). Treatment with KRAS-targeting siRNA alone had limited cytotoxicity across the tested concentrations (10 nM: 75% ± 4.7%, 50 nM: 82% ± 6.5%, 100 nM: 78% ± 7.6%).

However, combining free PTX and siRNA significantly enhanced therapeutic outcomes. The co-treatment at 50 nM PTX + 10 nM siRNA reduced viability to 49% (±1.9%), notably lower than either agent alone. At higher doses, combination treatments further decreased cell viability, achieving 26% (±5.4%) at 100 nM PTX + 50 nM siRNA, and as low as 16% (±7.1%) at 100 nM PTX + 100 nM siRNA, highlighting a clear synergistic or additive effect.

Importantly, CP-PTX-KRAS siRNA NPs further improved therapeutic efficacy compared to the free-drug combinations, likely due to enhanced co-delivery efficiency. At comparable concentrations, NPs significantly decreased viability to 46% (±4.2%) at 50 nM PTX + 10 nM siRNA, 23% (±5.8%) at 100 nM PTX + 50 nM siRNA, and reached just 11% (±8.1%) viability at the highest tested concentrations (200 nM PTX + 100 nM siRNA).

Collectively, these results indicate significant synergy between PTX-induced cytotoxicity and KRAS siRNA-mediated oncogene suppression, particularly when co-delivered via NPs, and highlight the potential therapeutic advantage of CP-PTX-KRAS siRNA NPs for pancreatic cancer treatment.

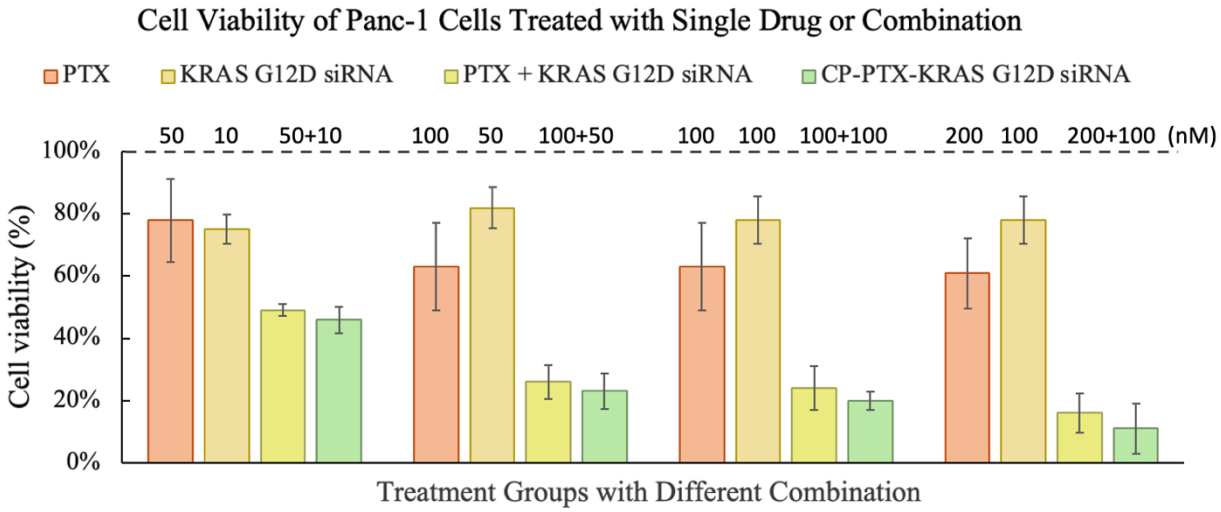

Figure 9. Cell viability across groups with varying concentrations of PTX and KRAS siRNA in PANC-1 Cells after 72 hours of incubation. PANC-1 cells were seeded in a 96-well plate (1×10^4 cells/well) and cultured for 24 hours prior to treatment. Cells were then treated with PTX, Lipo-siRNA, PTX combined with Lipo-siRNA, or CP-PTX-siRNA at different concentration combinations and incubated for 72 hours.

3.7.1 Dose-Response Analysis of KRAS G12D siRNA and PTX in PANC-1 Cells

To evaluate the cytotoxic effects of KRAS G12D-targeting siRNA and PTX in pancreatic cancer cells, PANC-1 cells were treated with increasing concentrations of each agent for 72 hours, followed by assessment of cell viability using the Alamar Blue assay. Viability values were normalized to untreated controls and analyzed using four-parameter nonlinear regression (**Figure 10**).

Treatment with KRAS G12D siRNA resulted in a concentration-dependent decrease in cell viability, with a calculated IC50 of 0.2784 μM and a Hill slope of –1.689 ($R^2 = 0.9655$), indicating a steep and dose-sensitive inhibitory response (63). In comparison, PTX treatment yielded a similar IC50 of 0.5470 μM, with a Hill slope of –0.3581 ($R^2 = 0.9838$). However, the upper asymptote (Top) and confidence intervals for the PTX curve were poorly constrained, suggesting potential parameter instability due to limited viability recovery at lower drug concentrations.

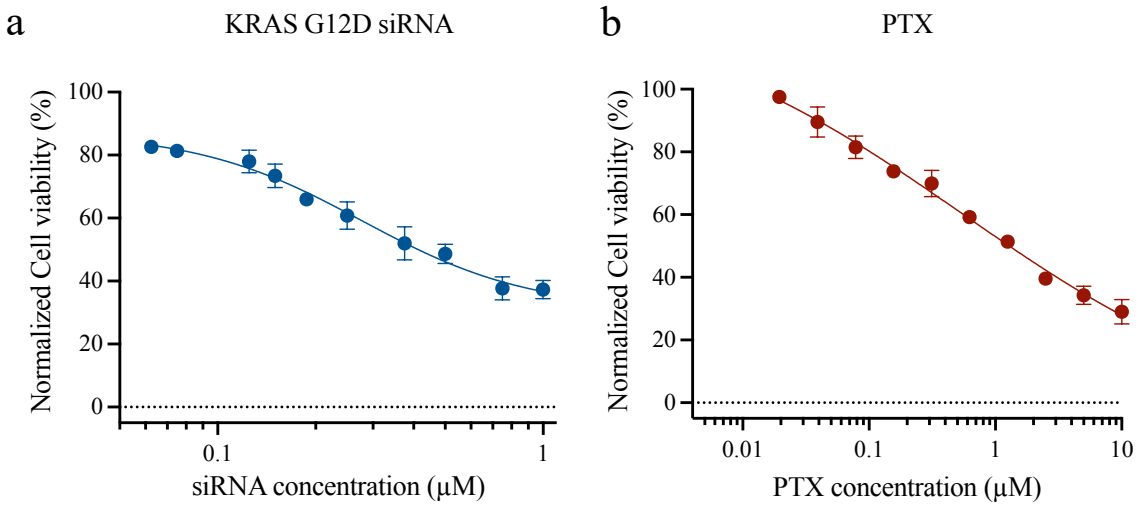

Figure 10. Dose-response curves of KRAS G12D siRNA and PTX in PANC-1 cells following 72-hour treatment. PANC-1 cells were treated with increasing concentrations of either (**a**) KRAS G12D-targeting siRNA or (**b**) PTX for 72 hours, and cell viability was assessed using the Alamar Blue assay. Data represent mean ± standard deviation (SD) from triplicate wells at each concentration. Viability values were normalized to untreated controls and analyzed using a four-parameter regression model in GraphPad Prism.

3.7.2 Ratio-dependent Cytotoxic Effects of PTX and KRAS G12D siRNA in PANC-1 Cells

To evaluate whether the co-treatment of KRAS G12D-targeting siRNA enhances cytotoxicity compared to single-agent treatments, PANC-1 cells were treated with free drug combinations at fixed PTX:siRNA molar ratios (1:0.2, 1:0.5, 1:1, and 1:2). Cells were incubated for 72 hours, and cell viability was measured using the Alamar Blue assay. Dose–response curves were generated by varying siRNA concentration, with PTX scaled proportionally based on each fixed ratio.

All drug combinations produced dose-dependent reductions in cell viability. The 1:0.2 combination exhibited the greatest potency, achieving an IC50 of 0.02176 µM based on siRNA and 0.1110 µM based on PTX. Other ratios yielded siRNA-based IC50 values of 0.02297 µM (1:0.5), 0.06172 µM (1:1), and 0.07195 µM (1:2), with corresponding PTX IC50 values of 0.04692 µM, 0.03629 µM, and 0.03541 µM, respectively. Although the 1:2 ratio had the lowest siRNA-based IC50, its PTX IC50 was higher than the 1:1 and 1:0.5 ratios, suggesting a shift in delivery efficiency when siRNA is in excess.

Nonlinear regression analysis showed good fit across all ratios, with R^2 values ranging from 0.93 to 0.98. Some fits showed unstable upper or lower asymptotes, indicated by wide confidence intervals and poorly defined span, potentially reflecting dose recovery variability or altered drug interaction (**Figure 11**). Steep Hill slopes (–6.1 to –18.5) suggested cooperative cytotoxic responses.

Combination index (CI) analysis was performed first to quantitatively assess drug interactions between PTX and siRNA, providing a standardized metric to distinguish between synergistic, additive, or antagonistic effects. This method, based on the Chou–Talalay median-effect principle, is widely used in evaluating combination therapy and allows direct comparison across different molar ratios and formulations (64). CI analysis confirmed synergistic interactions for all tested ratios. The greatest synergy occurred at 1:0.2 (CI = 0.4915), with moderate synergy also observed at 1:2 (CI = 0.5745), 1:1 (CI = 0.6009), and 1:0.5 (CI = 0.6479).

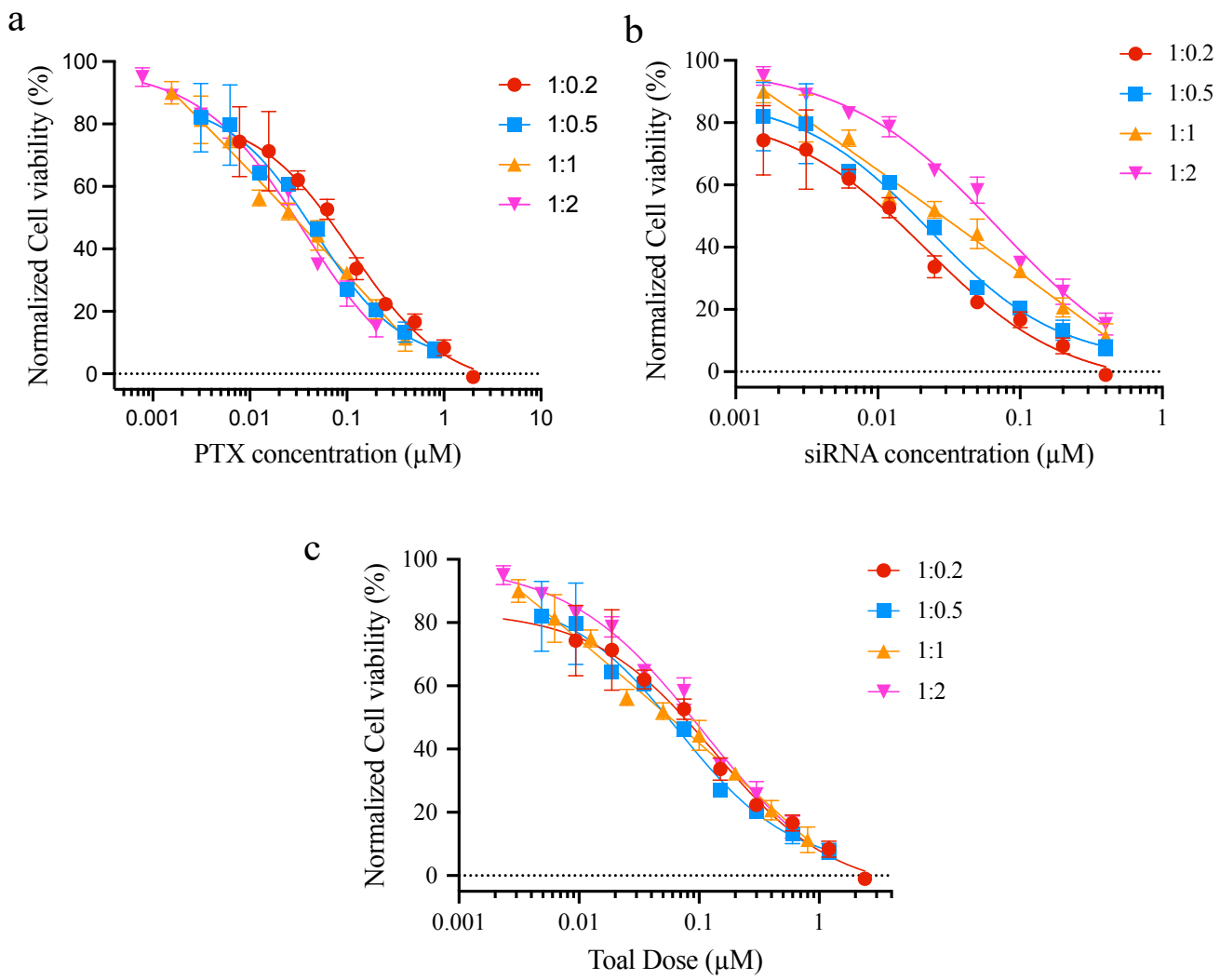

Figure 11. Dose–response curves of free drug combinations of PTX and KRAS G12D-targeting siRNA in PANC-1 cells at varying PTX:siRNA molar ratios. PANC-1 cells were treated with free PTX and siRNA mixtures at fixed molar ratios (1:0.2, 1:0.5, 1:1, 1:2) for 72 hours. Cell viability was assessed using the Alamar Blue assay and normalized to untreated controls. (**a**) Normalized cell viability plotted against PTX concentration (μM). (**b**) The same data plotted against siRNA concentration (μM), with PTX concentrations scaled proportionally according to each fixed molar ratio. (**c**) The same data plotted against total dose concentration (μM), Values were normalized to untreated controls. Data points represent mean ± standard deviation (SD) from triplicate wells.

3.7.3 Ratio-dependent Cytotoxic Effects of CP-PTX-KRAS G12D siRNA NPs in PANC-1 Cells

To determine whether NPs co-delivery of PTX and KRAS G12D-targeting siRNA enhances cytotoxicity relative to single-agent and free-drug combinations, PANC-1 cells were treated with CP-PTX-siRNA NPs at fixed PTX:siRNA molar ratios (1:0.2, 1:0.5, 1:1, and 1:2).

All tested NPs formulations induced potent, ratio-dependent cytotoxic effects. The 1:0.2 ratio achieved the greatest potency, with a total IC50 of 0.0921 μM, corresponding to 0.07825 μM PTX and 0.01389 μM siRNA. Other ratios showed similar or slightly reduced potency: IC50 values were 0.0344 μM (1:0.5), 0.0425 μM (1:1), and 0.0651 μM (1:2), based on total dose. All four formulations yielded well-fitted dose–response curves ($R^2 > 0.94$), with steep Hill slopes and minimal residual variability, indicating consistent cytotoxic behavior (**Figure 12**).

Compared to single-agent treatments, CP-PTX-siRNA NPs demonstrated marked improvements in potency. IC50 values for PTX and siRNA alone were 0.5470 μM and 0.2784 μM, respectively—over 6–15× higher than those of the most efficient NPs formulations. This highlights the enhanced intracellular delivery and pharmacodynamic synergy enabled by the NPs system.

Relative to free-drug combinations, CP-PTX-siRNA NPs also improved dose efficiency. For example, the free 1:0.2 combination had a total IC50 of 0.1328 μM, while the NPs achieved comparable efficacy at a total dose of 0.0921 μM. Similar trends were observed at the other ratios, with NPs delivery generally requiring lower doses to achieve 50% inhibition.

Combination index (CI) analysis further confirmed synergy in all NPs' formulations. The strongest synergy was observed at the 1:0.2 ratio (CI = 0.317), followed by 1:0.5 (CI = 0.386), 1:1 (CI = 0.449), and 1:2 (CI = 0.477). These CI values were consistently lower than or comparable to those from free-drug combinations, suggesting that CP-mediated co-delivery promotes more efficient and synergistic cytotoxicity in KRAS-mutant PANC-1 cells.

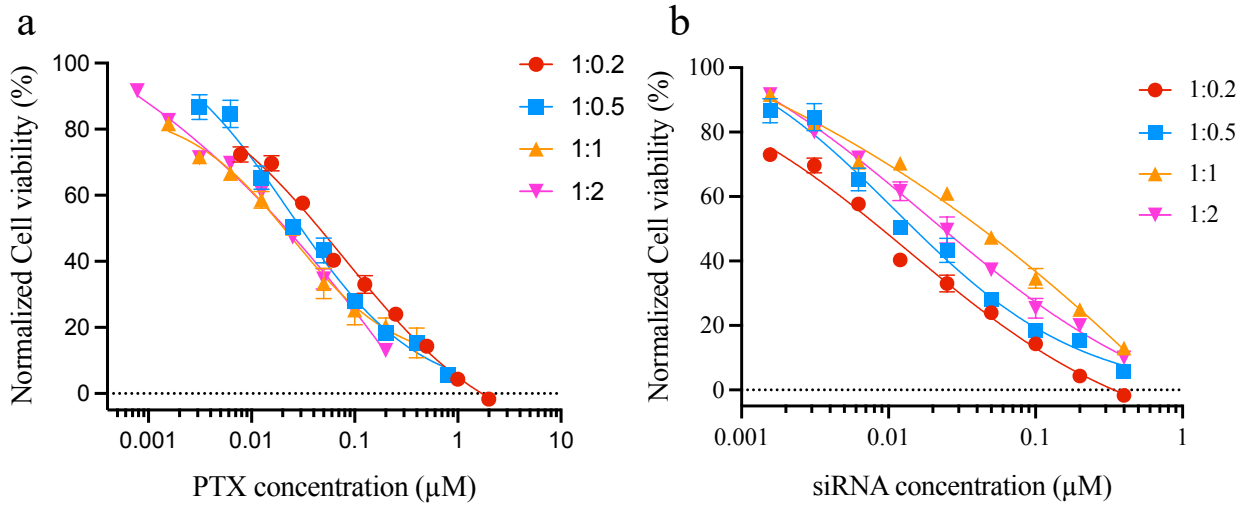

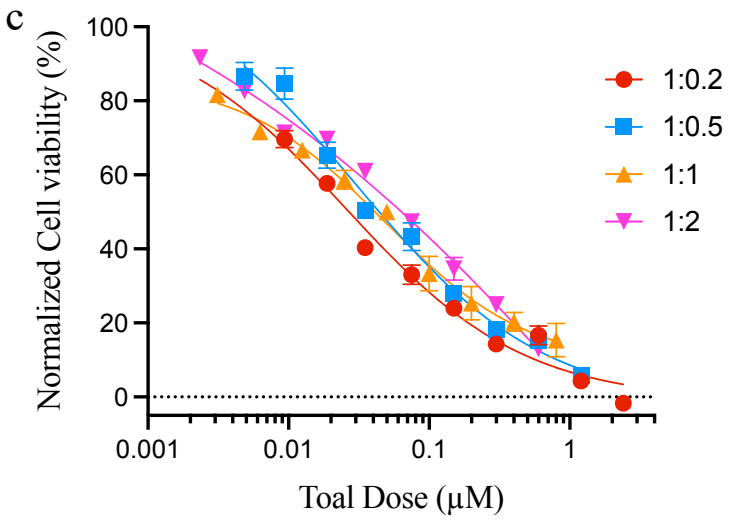

Figure 12. Dose–response curves showing the viability of PANC-1 cells treated with CP-PTX-KRAS G12D siRNA NPs at fixed PTX:siRNA molar ratios (1:0.2, 1:0.5, 1:1, 1:2). Viability was measured after 72 hours using the Alamar Blue assay and normalized to untreated controls. (**a**) Normalized cell viability plotted against PTX concentration (µM). (**b**) The same data plotted against siRNA concentration (µM), with PTX concentrations scaled proportionally according to each fixed molar ratio. (**c**) The same data plotted against total dose concentration (µM), Values were normalized to untreated controls. Data points represent mean ± standard deviation (SD) from triplicate wells.

Table 1. Combination Index (CI) values of PTX and siRNA administered either as admix drug co-treatment or as CP-PTX-siRNA NPs at varying PTX:siRNA molar ratios (1:0.2, 1:0.5, 1:1, and 1:2). For each combination, the IC_{50}-equivalent concentrations of PTX and siRNA were used to compute CI values based on the Chou–Talalay method (64).

PTX:siRNA Ratio	Formulation	PTX (µM)	siRNA (µM)	Total dose (µM)	CI Value	Interpretation
PTX only	Free drug	0.5470	-	-	-	-
siRNA only	Free drug	-	0.2784	-	-	-
1:0.2	Free drug	0.1110	0.02176	0.1328	0.400	Synergy
	NPs	0.07825	0.01389	0.0921	0.317	Synergy
1:0.5	Free drug	0.04692	0.02297	0.0699	0.506	Synergy
	NPs	0.02331	0.01113	0.0344	0.386	Synergy
1:1	Free drug	0.03629	0.06172	0.0980	0.668	Synergy
	NPs	0.02412	0.01842	0.0425	0.449	Synergy
1:2	Free drug	0.03541	0.07195	0.1074	0.684	Synergy
	NPs	0.04672	0.01842	0.0651	0.477	Synergy

4. Conclusion

This study demonstrates the successful development and application of a modular NP platform, CP-PTX-siRNA, for the co-delivery of PTX and KRAS G12D-targeting siRNA in pancreatic cancer cells. We were able to first modify PTX with succinic anhydride to form PTX-COOH, which enables pH-responsive conjugation to chitosan–PEG (CP) via EDC/NHS chemistry. The resulting CP-PTX conjugate was confirmed by ^{1}H NMR, with a drug loading efficiency of ~3.21 wt%. CP-PTX NPs were then evaluated for nucleic acid complexation. CP-PTX was firstly complexed with PolyIC with the optimal formulation at a CP-PTX:PolyIC ratio of 11:1 (+4.1 mV). With a procedure optimized from PolyIC loading, KRAS G12D siRNA was complexed with CP-PTX through a simple sonication process. The optimal 1:0.1 CP-PTX:siRNA formulation yielded particles averaging 26.47 nm with a zeta potential of –9.76 mV.

Initial validation in Pan02-Luc cells using luciferase siRNA confirmed that the CP-PTX carrier maintained the cytotoxic activity of PTX while enabling effective siRNA delivery and gene knockdown. When applied to KRAS-mutant PANC-1 cells, CP-PTX-siRNA NPs exhibited robust and dose-dependent cytotoxicity across a range of PTX:siRNA molar ratios. Among tested ratios, the 1:0.2 NPs formulation exhibited the highest potency, achieving IC50 values of 0.0783 μM PTX and 0.0139 μM siRNA, significantly lower compared to individual treatments (free PTX IC50 = 0.5470 μM; free siRNA IC50 = 0.2784 μM).

Importantly, all CP-PTX-siRNA combinations exhibited combination index (CI) values below 1.0, indicating clear synergistic interactions. The most pronounced synergy was observed with the 1:0.2 NPs formulation (CI = 0.317), which surpassed the synergy of corresponding admix drug co-treatments (CI = 0.400). NP-mediated co-delivery consistently achieved enhanced cytotoxic effects at substantially reduced total doses compared to free drug combinations, highlighting the significant therapeutic advantage of synchronized chemo-gene delivery.

Collectively, our findings establish CP-PTX-siRNA as an effective dual-functional platform for chemo–gene therapy in KRAS-driven pancreatic cancer. This biocompatible and tunable system not only enhances the potency of conventional chemotherapy but also enables the delivery of gene-silencing therapeutics. These results support further preclinical evaluation of CP-PTX-siRNA for *in vivo* application and potential clinical translation.

5. References

1. Siegel RL, Kratzer TB, Giaquinto AN, Sung H, Jemal A. Cancer statistics, 2025. CA Cancer J Clin. 2025;75(1):10-45.
2. Qin Q, Yu R, Eriksson JE, Tsai HI, Zhu H. Cancer-associated fibroblasts in pancreatic ductal adenocarcinoma therapy: Challenges and opportunities. Cancer Lett. 2024;591:216859.
3. Waddell N, Pajic M, Patch AM, Chang DK, Kassahn KS, Bailey P, et al. Whole genomes redefine the mutational landscape of pancreatic cancer. Nature. 2015;518(7540):495-501.
4. Stefanoudakis D, Frountzas M, Schizas D, Michalopoulos NV, Drakaki A, Toutouzas KG. Significance of TP53, CDKN2A, SMAD4 and KRAS in Pancreatic Cancer. Curr Issues Mol Biol. 2024;46(4):2827-44.
5. Kamisawa T, Wood LD, Itoi T, Takaori K. Pancreatic cancer. Lancet. 2016;388(10039):73-85.
6. Truong LH, Pauklin S. Pancreatic Cancer Microenvironment and Cellular Composition: Current Understandings and Therapeutic Approaches. Cancers (Basel). 2021;13(19).
7. Monteran L, Erez N. The Dark Side of Fibroblasts: Cancer-Associated Fibroblasts as Mediators of Immunosuppression in the Tumor Microenvironment. Front Immunol. 2019;10:1835.
8. Sarantis P, Koustas E, Papadimitropoulou A, Papavassiliou AG, Karamouzis MV. Pancreatic ductal adenocarcinoma: Treatment hurdles, tumor microenvironment and immunotherapy. World J Gastrointest Oncol. 2020;12(2):173-81.
9. Nusrat F, Khanna A, Jain A, Jiang W, Lavu H, Yeo CJ, et al. The Clinical Implications of KRAS Mutations and Variant Allele Frequencies in Pancreatic Ductal Adenocarcinoma. J Clin Med. 2024;13(7).
10. Mondal K, Posa MK, Shenoy RP, Roychoudhury S. KRAS Mutation Subtypes and Their Association with Other Driver Mutations in Oncogenic Pathways. Cells. 2024;13(14).
11. Prior IA, Hood FE, Hartley JL. The Frequency of Ras Mutations in Cancer. Cancer Res. 2020;80(14):2969-74.
12. Fruman DA, Chiu H, Hopkins BD, Bagrodia S, Cantley LC, Abraham RT. The PI3K Pathway in Human Disease. Cell. 2017;170(4):605-35.
13. Liu C, Zheng S, Wang Z, Wang S, Wang X, Yang L, et al. KRAS-G12D mutation drives immune suppression and the primary resistance of anti-PD-1/PD-L1 immunotherapy in non-small cell lung cancer. Cancer Commun (Lond). 2022;42(9):828-47.
14. Canon J, Rex K, Saiki AY, Mohr C, Cooke K, Bagal D, et al. The clinical KRAS(G12C) inhibitor AMG 510 drives anti-tumour immunity. Nature. 2019;575(7781):217-23.
15. Waters AM, Der CJ. KRAS: The Critical Driver and Therapeutic Target for Pancreatic Cancer. Cold Spring Harb Perspect Med. 2018;8(9).
16. Hallin J, Bowcut V, Calinisan A, Briere DM, Hargis L, Engstrom LD, et al. Anti-tumor efficacy of a potent and selective non-covalent KRAS(G12D) inhibitor. Nat Med. 2022;28(10):2171-82.
17. Kleeff J, Korc M, Apte M, La Vecchia C, Johnson CD, Biankin AV, et al. Pancreatic cancer. Nat Rev Dis Primers. 2016;2:16022.
18. Conroy T, Desseigne F, Ychou M, Bouche O, Guimbaud R, Becouarn Y, et al. FOLFIRINOX versus gemcitabine for metastatic pancreatic cancer. N Engl J Med. 2011;364(19):1817-25.

19. Von Hoff DD, Ervin T, Arena FP, Chiorean EG, Infante J, Moore M, et al. Increased survival in pancreatic cancer with nab-paclitaxel plus gemcitabine. N Engl J Med. 2013;369(18):1691-703.
20. Frese KK, Neesse A, Cook N, Bapiro TE, Lolkema MP, Jodrell DI, Tuveson DA. nab-Paclitaxel potentiates gemcitabine activity by reducing cytidine deaminase levels in a mouse model of pancreatic cancer. Cancer Discov. 2012;2(3):260-9.
21. Wong W, Raufi AG, Safyan RA, Bates SE, Manji GA. BRCA Mutations in Pancreas Cancer: Spectrum, Current Management, Challenges and Future Prospects. Cancer Manag Res. 2020;12:2731-42.
22. van Asperen CJ, Brohet RM, Meijers-Heijboer EJ, Hoogerbrugge N, Verhoef S, Vasen HF, et al. Cancer risks in BRCA2 families: estimates for sites other than breast and ovary. J Med Genet. 2005;42(9):711-9.
23. Feig C, Gopinathan A, Neesse A, Chan DS, Cook N, Tuveson DA. The pancreas cancer microenvironment. Clin Cancer Res. 2012;18(16):4266-76.
24. Ino Y, Yamazaki-Itoh R, Shimada K, Iwasaki M, Kosuge T, Kanai Y, Hiraoka N. Immune cell infiltration as an indicator of the immune microenvironment of pancreatic cancer. Br J Cancer. 2013;108(4):914-23.
25. Torphy RJ, Zhu Y, Schulick RD. Immunotherapy for pancreatic cancer: Barriers and breakthroughs. Ann Gastroenterol Surg. 2018;2(4):274-81.
26. Longhi MP, Trumpfheller C, Idoyaga J, Caskey M, Matos I, Kluger C, et al. Dendritic cells require a systemic type I interferon response to mature and induce CD4+ Th1 immunity with poly IC as adjuvant. J Exp Med. 2009;206(7):1589-602.
27. Stahl-Hennig C, Eisenblatter M, Jasny E, Rzehak T, Tenner-Racz K, Trumpfheller C, et al. Synthetic double-stranded RNAs are adjuvants for the induction of T helper 1 and humoral immune responses to human papillomavirus in rhesus macaques. PLoS Pathog. 2009;5(4):e1000373.
28. Kawai T, Akira S. Toll-like receptor and RIG-I-like receptor signaling. Ann N Y Acad Sci. 2008;1143:1-20.
29. Trumpfheller C, Caskey M, Nchinda G, Longhi MP, Mizenina O, Huang Y, et al. The microbial mimic poly IC induces durable and protective CD4+ T cell immunity together with a dendritic cell targeted vaccine. Proc Natl Acad Sci U S A. 2008;105(7):2574-9.
30. McBride S, Hoebe K, Georgel P, Janssen E. Cell-associated double-stranded RNA enhances antitumor activity through the production of type I IFN. J Immunol. 2006;177(9):6122-8.
31. Cox AD, Fesik SW, Kimmelman AC, Luo J, Der CJ. Drugging the undruggable RAS: Mission possible? Nat Rev Drug Discov. 2014;13(11):828-51.
32. Moore AR, Rosenberg SC, McCormick F, Malek S. RAS-targeted therapies: is the undruggable drugged? Nat Rev Drug Discov. 2020;19(8):533-52.
33. Strand MS, Krasnick BA, Pan H, Zhang X, Bi Y, Brooks C, et al. Precision delivery of RAS-inhibiting siRNA to KRAS driven cancer via peptide-based nanoparticles. Oncotarget. 2019;10(46):4761-75.
34. Kang H, Ga YJ, Kim SH, Cho YH, Kim JW, Kim C, Yeh JY. Small interfering RNA (siRNA)-based therapeutic applications against viruses: principles, potential, and challenges. J Biomed Sci. 2023;30(1):88.
35. Van Cutsem E, Collignon J, Eefsen RL, Ochsenreither S, Zvirbule Z, Ivanauskas A, et al. Efficacy and Safety of the Anti-IL1RAP Antibody Nadunolimab (CAN04) in Combination with

Gemcitabine and Nab-Paclitaxel in Patients with Advanced/Metastatic Pancreatic Cancer. Clin Cancer Res. 2024;30(23):5293-303.
36. Grierson PM, Tan B, Pedersen KS, Park H, Suresh R, Amin MA, et al. Phase Ib Study of Ulixertinib Plus Gemcitabine and Nab-Paclitaxel in Patients with Metastatic Pancreatic Adenocarcinoma. Oncologist. 2023;28(2):e115-e23.
37. Golan T, Hammel P, Reni M, Van Cutsem E, Macarulla T, Hall MJ, et al. Maintenance Olaparib for Germline BRCA-Mutated Metastatic Pancreatic Cancer. N Engl J Med. 2019;381(4):317-27.
38. Venturoli D, Rippe B. Ficoll and dextran vs. globular proteins as probes for testing glomerular permselectivity: effects of molecular size, shape, charge, and deformability. Am J Physiol Renal Physiol. 2005;288(4):F605-13.
39. Decuzzi P, Pasqualini R, Arap W, Ferrari M. Intravascular delivery of particulate systems: does geometry really matter? Pharm Res. 2009;26(1):235-43.
40. Al-Thani AN, Jan AG, Abbas M, Geetha M, Sadasivuni KK. Nanoparticles in cancer theragnostic and drug delivery: A comprehensive review. Life Sci. 2024;352:122899.
41. Yu B, Tai HC, Xue W, Lee LJ, Lee RJ. Receptor-targeted nanocarriers for therapeutic delivery to cancer. Mol Membr Biol. 2010;27(7):286-98.
42. Nguyen PV, Allard-Vannier E, Chourpa I, Herve-Aubert K. Nanomedicines functionalized with anti-EGFR ligands for active targeting in cancer therapy: Biological strategy, design and quality control. Int J Pharm. 2021;605:120795.
43. Suk JS, Xu Q, Kim N, Hanes J, Ensign LM. PEGylation as a strategy for improving nanoparticle-based drug and gene delivery. Adv Drug Deliv Rev. 2016;99(Pt A):28-51.
44. Yang Q, Jones SW, Parker CL, Zamboni WC, Bear JE, Lai SK. Evading immune cell uptake and clearance requires PEG grafting at densities substantially exceeding the minimum for brush conformation. Mol Pharm. 2014;11(4):1250-8.
45. Chehelgerdi M, Chehelgerdi M, Allela OQB, Pecho RDC, Jayasankar N, Rao DP, et al. Progressing nanotechnology to improve targeted cancer treatment: overcoming hurdles in its clinical implementation. Mol Cancer. 2023;22(1):169.
46. Sun L, Li Z, Lan J, Wu Y, Zhang T, Ding Y. Better together: nanoscale co-delivery systems of therapeutic agents for high-performance cancer therapy. Front Pharmacol. 2024;15:1389922.
47. Ouyang P, Wang L, Wu J, Tian Y, Chen C, Li D, et al. Overcoming cold tumors: a combination strategy of immune checkpoint inhibitors. Front Immunol. 2024;15:1344272.
48. Li J, Cai C, Li J, Li J, Li J, Sun T, et al. Chitosan-Based Nanomaterials for Drug Delivery. Molecules. 2018;23(10).
49. Shukla SK, Mishra AK, Arotiba OA, Mamba BB. Chitosan-based nanomaterials: a state-of-the-art review. Int J Biol Macromol. 2013;59:46-58.
50. Fernandes JC, Qiu X, Winnik FM, Benderdour M, Zhang X, Dai K, Shi Q. Low molecular weight chitosan conjugated with folate for siRNA delivery in vitro: optimization studies. Int J Nanomedicine. 2012;7:5833-45.
51. Desai N, Rana D, Salave S, Gupta R, Patel P, Karunakaran B, et al. Chitosan: A Potential Biopolymer in Drug Delivery and Biomedical Applications. Pharmaceutics. 2023;15(4).
52. Quinones JP, Peniche H, Peniche C. Chitosan Based Self-Assembled Nanoparticles in Drug Delivery. Polymers (Basel). 2018;10(3).
53. Dimassi S, Tabary N, Chai F, Blanchemain N, Martel B. Sulfonated and sulfated chitosan derivatives for biomedical applications: A review. Carbohydr Polym. 2018;202:382-96.

54. Hasanbegloo K, Banihashem S, Faraji Dizaji B, Bybordi S, Farrokh-Eslamlou N, Abadi PG, et al. Paclitaxel-loaded liposome-incorporated chitosan (core)/poly(epsilon-caprolactone)/chitosan (shell) nanofibers for the treatment of breast cancer. Int J Biol Macromol. 2023;230:123380.
55. Ding J, Guo Y. Recent Advances in Chitosan and its Derivatives in Cancer Treatment. Front Pharmacol. 2022;13:888740.
56. Lee E, Lee J, Lee IH, Yu M, Kim H, Chae SY, Jon S. Conjugated chitosan as a novel platform for oral delivery of paclitaxel. J Med Chem. 2008;51(20):6442-9.
57. Veiseh O, Sun C, Fang C, Bhattarai N, Gunn J, Kievit F, et al. Specific targeting of brain tumors with an optical/magnetic resonance imaging nanoprobe across the blood-brain barrier. Cancer Res. 2009;69(15):6200-7.
58. Mu Q, Lin G, Stephen ZR, Chung S, Wang H, Patton VK, et al. In vivo Serum Enabled Production of Ultrafine Nanotherapeutics for Cancer Treatment. Mater Today (Kidlington). 2020;38:10-23.
59. Jiang W, Li H, Liu X, Zhang J, Zhang W, Li T, et al. Precise and efficient silencing of mutant Kras(G12D) by CRISPR-CasRx controls pancreatic cancer progression. Theranostics. 2020;10(25):11507-19.
60. Huang J, Chien YT, Mu Q, Zhang M. An Efficient Fabrication Approach for Multi-Cancer Responsive Chemoimmuno Co-Delivery Nanoparticles. Pharmaceutics. 2024;16(10).
61. Wei Y, Quan L, Zhou C, Zhan Q. Factors relating to the biodistribution & clearance of nanoparticles & their effects on in vivo application. Nanomedicine (Lond). 2018;13(12):1495-512.
62. Pham TND, Shields MA, Spaulding C, Principe DR, Li B, Underwood PW, et al. Preclinical Models of Pancreatic Ductal Adenocarcinoma and Their Utility in Immunotherapy Studies. Cancers (Basel). 2021;13(3).
63. Prinz H. Hill coefficients, dose-response curves and allosteric mechanisms. J Chem Biol. 2010;3(1):37-44.
64. Chou TC. Drug combination studies and their synergy quantification using the Chou-Talalay method. Cancer Res. 2010;70(2):440-6.